AD-A137 879 CHEMICAL REACTIONS AND MOLECULAR AGGREGATION IN CRYOGENIC WHOLE AIR SAMPL.. (U) BROWN UNIV PROVIDENCE RI DIV OF ENGINEERING J M CALO ET AL. JUL 83 1/2

UNCLASSIFIED AFGL-TR-83-0235 F19628-81-C-0157 F/G 4/1 NL

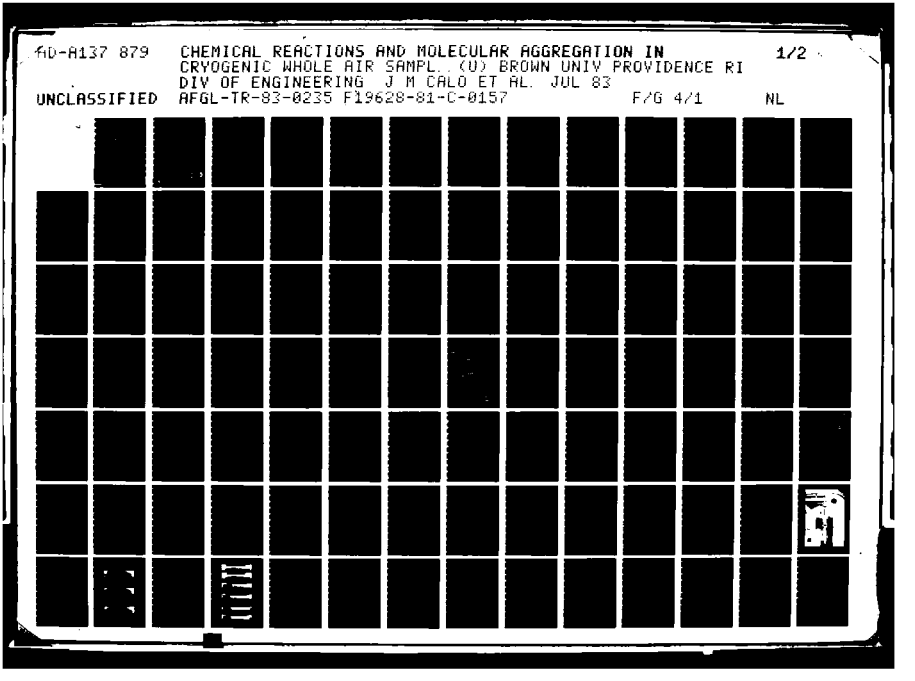

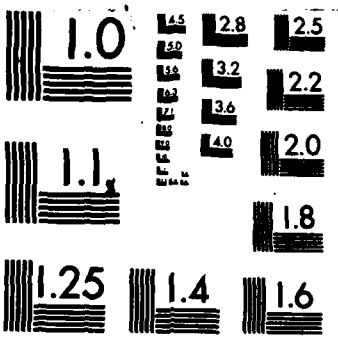

MICROCOPY RESOLUTION TEST CHART
NATIONAL BUREAU OF STANDARDS-1963-A

AFGL-TR-83-0235

CHEMICAL REACTIONS AND MOLECULAR AGGREGATION IN CRYOGENIC WHOLE AIR SAMPLE MATRICES

J.M. Calo
W.D. Lilly

Division of Engineering
Brown University
Providence, Rhode Island 02912

Final Report
1 October 1981 - 31 March 1983

July 1983

Approved for public release; distribution unlimited.

AIR FORCE GEOPHYSICS LABORATORY
AIR FORCE SYSTEMS COMMAND
UNITED STATES AIR FORCE
HANSCOM AFB, MASSACHUSETTS 01731

This report has been reviewed by the ESD Public Affairs Office (PA) and is releasable to the National Technical Information Service (NTIS).

This technical report has been reviewed and is approved for publication

Charles C. Gallagher

Contract Manager

Branch Chief

FOR THE COMMANDER

C. J. Sterzer

Division Director

Qualified requestors may obtain additional copies from the Defense Technical Information Center. All others should apply to the National Technical Information Service.

If your address has changed, or if you wish to be removed from the mailing list, or if the addressee is no longer employed by your organization, please notify AFGL/DAA, Hanscom AFB, MA 01731. This will assist us in maintaining a current mailing list.

Do not return copies of this report unless contractual obligations or notices on a specific document requires that it be returned.

Unclassified

SECURITY CLASSIFICATION OF THIS PAGE (When Data Entered)

REPORT DOCUMENTATION PAGE		READ INSTRUCTIONS BEFORE COMPLETING FORM
1. REPORT NUMBER AFGL-TR-83-0235	2. GOVT ACCESSION NO. AD-A137879	3. RECIPIENT'S CATALOG NUMBER
4. TITLE (and Subtitle) Chemical Reactions and Molecular Aggregation in Cryogenic Whole Air Sample Matrices		5. TYPE OF REPORT & PERIOD COVERED Final Report for Period 1 Oct. 1981 - 31 March 1983 6. PERFORMING ORG. REPORT NUMBER
7. AUTHOR(s) J. M. Calo and W. D. Lilly		8. CONTRACT OR GRANT NUMBER(s) F19628-81-C-0157
9. PERFORMING ORGANIZATION NAME AND ADDRESS Division of Engineering BROWN UNIVERSITY Providence, R. I. 02912		10. PROGRAM ELEMENT, PROJECT, TASK AREA & WORK UNIT NUMBERS 62101F, 668703AR
11. CONTROLLING OFFICE NAME AND ADDRESS Air Force Geophysics Laboratory Hanscom AFB, MA 01731 Monitor/Charles C. Gallagher/LKD		12. REPORT DATE July 1983 13. NUMBER OF PAGES 118
14. MONITORING AGENCY NAME & ADDRESS(if different from Controlling Office)		15. SECURITY CLASS. (of this report) UNCLAS 15a. DECLASSIFICATION/DOWNGRADING SCHEDULE

16. DISTRIBUTION STATEMENT (of this Report)

"Approved for public release; distribution unlimited."

17. DISTRIBUTION STATEMENT (of the abstract entered in Block 20, if different from Report)

18. SUPPLEMENTARY NOTES

19. KEY WORDS (Continue on reverse side if necessary and identify by block number)

Cryogenic sampling of stratospheric gases; oxides of nitrogen and water vapor; infrared analysis of condensed samples.

20. ABSTRACT (Continue on reverse side if necessary and identify by block number)

This report conveys the results of an investigation concerned with the effects of chemical reactions in cryogenically condensed $NO_x/O_x/H_2O$ samples, on the alteration of sample composition upon subsequent thermal desorption. These studies were undertaken to elucidate the relevant mechanisms and improve the understanding of these processes as they relate to the analysis of cryogenically-collected stratospheric whole air samples acquired in the balloon-borne sampling project of the composition task of the Stratospheric

DD FORM 1 JAN 73 1473 EDITION OF 1 NOV 65 IS OBSOLETE
S/N 0102-LF-014-6601

20. continued

Environment Program of the Air Force Geophysics Laboratory.

An experimental apparatus was developed around a mechanical, closed-cycle, helium cryogenic refrigerator to perform the following functions: (1) condensed sample generation by controlled deposition from the gas phase onto the cryogenic surface; (2) in-situ observation via infrared transmission spectrophotometry; and (3) post-regeneration analysis of the thermally desorbed gas samples by NO_x chemiluminescence and/or gas chromatography. In addition, provision was made to vary the water vapor composition of the samples.

The major features of infrared spectra of condensed samples were interpreted in terms of assignments to the various species of importance. Subsequent experiments with $NO_x/O_x/H_2O$ samples substantiated that condensed NO self-disproportionates to a significant degree upon thermal regeneration. Furthermore, it was found that the intensity of the absorption peak indicative of NO_2 formation in the condensed sample was inversely proportional to the total amount of water in the sample, although the final conversion to NO_x upon thermal desorption remained approximately constant. This behavior was interpreted as an NO conversion mechanism involving the nitrogen oxyacids, nitrous and nitric acids, in the presence of large amounts of water in the condensed sample. This could not be directly proven since the infrared absorption features of the acids are obscured by the N-O and O-H features, and the two gas chromatographic column packings that were tried could not provide unambiguous separation of the acids. However, the fact that water does play a significant role in total NO conversion was shown in experiments including O_2 and O_3 in the condensed sample. In these experiments, the O_x was observed to convert NO to NO_2 in the condensed sample, which then presumably reacted readily to acids, resulting in significantly increased conversion to NO_x upon thermal desorption, over and above that measured for NO alone.

In addition to the infrared/NO_x chemiluminescence studies, separate sample immersion studies in liquid nitrogen and helium were conducted which permitted visual observations of the condensed samples upon warming. These studies qualitatively substantiated the other NO conversion results, and were used as an aid in understanding and interpreting the other experiments.

The results of this work indicate that interconversion of the oxides of nitrogen in condensed samples, especially in the presence of water vapor, is a significant process under certain conditions. However, additional work involving careful cryogenic deposition of very small amounts of the various species, combined with perhaps high resolution FTIR, is definitely needed in order to quantitatively assess the relative importance of these same processes in the much more highly dilute stratospheric cryogenic whole air samples.

TABLE OF CONTENTS

"Original contains color plates: All DTIC reproductions will be in black and white"

LIST OF TABLES

LIST OF FIGURES

1.0. INTRODUCTION.

The trace gas composition of the stratosphere has received significant attention since the initial impetus provided by the Climatic Impact Assessment Program of the Department of Transportation in the early 1970's. At that time it was suggested (Snelson, 1972) that cryogenic sampling of stratospheric air could be performed in such a manner as to exploit the inherent advantage of the high dilution of trace species in the frozen air matrix. Snelson (1972) noted that species present in concentrations of parts-per-million and lower would be imbedded in a matrix composed principally of nitrogen and oxygen. It was reasoned that this state of "matrix isolation" would tend to severely inhibit potential reactions due to extremely low temperatures and diffusion rates, thereby preserving reactive species. Potentially, many of these could be studied using in-situ techniques such as electron paramagnetic resonance (EPR), nuclear magnetic resonance (NMR), and spectroscopy. The measurement of other species, however, would necessitate the use of alternate analytical techniques such as gas chromatography (GC), chemiluminescence (for NO_x), and mass spectrometry (MS); all of which are destructive with respect to the solid matrix, requiring at least thermal desorption, and possibly other subsequent manipulations such as fractionation. Obviously, under these latter conditions the advantages of matrix isolation are lost, and there exists the possibility that the original sample composition will be altered.

In addition to the preceding problems with reactive species,

reactions between what may be considered to be relatively "stable" molecular species have also been observed in the solid phase; e.g., oxidation of nitric oxide by oxygen (Smith and Guillory, 1977, 1977a), and by ozone (Lucas, 1977, and Lucas and Pimentel, 1979). In addition, ozone is known to recombine in the condensed state under various conditions (sometimes explosively); e.g., see Deitz and Bitner, 1973, and Jenkins, 1959. In some of these studies recombination mechanisms involving catalytic impurities and/or oxidative chain reactions have been hypothesized (e.g., see Arin and Warneck, 1972, and Jenkins, 1959). Thus, thermal regeneration of these species, and mixtures thereof, may also lead to significant alteration of ambient relative compositions.

Since 1974 the Air Force Geophysics Laboratory has been conducting a research effort concerned with cryogenic whole air sampling of the stratosphere (Gallagher et al., 1981). In this program, fixed metal cylinders (three in the most recent configurations), with specially treated inner surfaces, are immersed in a liquid helium bath surrounded by a guard volume of liquid nitrogen. This "tri- whole air sampler" (TRIWAS) is the heart of a balloon flight package which is designed to collect one whole air sample per cylinder at different stratospheric altitudes, typically in the 12 to 30 km range. Once sampling is completed on the balloon descent leg of the flight, the sampler is parachuted to the ground where it is recovered and maintained at cryogenic temperatures until regeneration and gas analysis can be performed in the laboratory to determine relative ambient stratospheric composition.

Even though this program is relatively simple in concept, the many processes associated with the collection and regeneration of atmospheric gas mixtures onto and from cryogenic surfaces are not well understood. The very nature of multilayered deposits of atmospheric species on polycrystalline substrates, and their subsequent behavior upon warming and thermal desorption, including the effects of chemical reactions cited above, represent complex and interrelated physico-chemical phenomena.

This final report summarizes the work performed and the results of a study specifically focused on the effect of chemical reactions in solid cryogenic samples on alteration of relative compositions upon thermal regeneration. More specifically, the work concentrated on the investigation of the conversion of NO_x and O_x species and water vapor in cryofrost matrices using infrared spectrophotometry and NO_x chemiluminescence. In addition, visual observations of the thermal regeneration of cryogenic samples composed of these species were helpful in interpreting and understanding the various data.

2.0. EXPERIMENTAL

2.1. Overview.

A schematic of the apparatus developed for the current studies on cryogenic samples of $NO_x/O_x/H_2O$ mixtures is presented in Figure 1. The primary functions of this experimental system are: (1) sample generation: to allow controlled deposition of gas samples onto a cryogenic surface; (2) in-situ observation: to

obtain direct infrared transmission spectra of the condensed sample as a function of temperature; (3) post-regeneration analysis: to analyze desorbed gas phase samples by NO_x chemiluminescence. In addition, provision was made for auxiliary cryopumping for water vapor interaction studies. A more detailed description of the apparatus is given in Appendix A, and the general experimental procedures are described in Appendix B.

3.0. RESULTS AND DISCUSSION.

3.1. IR Spectrophotometry.

3.1-1. Peak Identification.

A series of spectra were taken of condensed samples of the various species expected to be involved in the work that follows for the purpose of identification and assignment of the absorption peaks.

3.1-1.1. Nitrous Oxide.

A typical spectrum of condensed nitrous oxide is presented in Figure 2. Nitrous oxide gas directly from the cylinder (Linde, minimum purity 97%) was deposited on the CdTe window in the manner described in Appendix B. The fundamental modes of N_2O in the condensed state are clearly evident; i.e., the stretching modes, ν_3 and ν_1, at 2200 and 1280 cm^{-1}, respectively (Hallam, 1973). (The expected N_2O bending mode at 585 cm^{-1} lies beyond the cutoff of the CaF_2 IR cell windows.) The other features are most probably combinations and overtones of the fundamentals, and/or unidentified impurities. Since N_2O was found to be relatively unimportant in the current work, no additional effort was expended in obtaining more detailed assignments.

All the absorption features remain unchanged as a function of time except for the broad absorption peak at approximately 3200 cm^{-1}. This feature continues to grow with time after deposition, even during heating of an N_2O sample to desorption, as shown in Figure 3. The N_2O sample disappears at ~100K with no obvious changes in the features already attributed to N_2O between 18K and 100K. The 3200 cm^{-1} feature, however, continues to grow to ~200K, where it abruptly disappears.

A typical background spectrum with the sample window cold (16K) with no condensed gas sample is presented in Figure 4 for comparison. It is quite obvious that this spectrum also exhibits the 3200 cm^{-1} feature, and it behaves in the same manner as in the N_2O condensed sample spectra; i.e., it steadily increases with time at low temperatures, disappearing entirely at relatively high temperatures (~200K). Thus, this feature is definitely not due to N_2O, but rather is indicative of additional accumulation of the species responsible over the time span of an experiment as a result of continual deposition from the gas phase. It is believed that the 3200 cm^{-1} absorption feature is due to background water vapor accumulating and polymerizing on the sample window. This absorption lies in the correct region of the strong fundamental O-H stretching frequencies. A similar absorption has been observed for hydrogen-bonded species with OH groups in polymerized form in condensed phases (e.g., see Bellamy, 1975). In addition, the disappearance temperature of this feature (i.e., ~200K) is indicative of water condensate desorption in vacuo (e.g., see Calo et al., 1981).

3.1-1.2. Nitric Oxide.

A typical spectrum of condensed nitric oxide is presented in Figure 5. Nitric oxide gas directly from the cylinder (Linde, 98.5% minimum purity) was deposited on the CdTe sample window in the manner described in Appendix B. Clearly evident are the two strong absorptions at 1845 and 1740 cm^{-1}. The appearance of these features strongly resembles the spectrum of approximately 0.17 mol fraction NO in N_2 given by Smith et al. (1951) (reproduced as Figure 8), who examined the infrared and Raman spectra of solid and liquid nitric oxide. As shown in both Figures 5 and 8, the higher frequency feature is quite sharp, and the lower frequency one appears split into a doublet. Smith et al. (1951) attributed both absorptions to the NO dimer. The higher frequency peak was attributed to symmetric stretch, and the lower frequency to asymmetric stretch. It was also speculated that the splitting evident in the 1770 cm^{-1} peak was possibly due to the coexistence of two types of dimer. However, in infrared studies of NO isolated in a solid oxygen matrix, Smith and Guillory (1977) observed only one form of the NO dimer, and assigned peaks at 1861 and 1773 cm^{-1} to the cis-$(NO)_2$ dimer (see Figure 9). These workers also assigned a strong absorption at 1866 cm^{-1} to monomeric NO (see Figure 9), and point out that, "This feature is close to, if somewhat lower than, those observed for NO trapped in solid N_2 (Guillory and Hunter, 1969; Varetti and Pimentel, 1971) (1878 cm^{-1}), or solid Ar (Fateley et al., 1959) (1875 cm^{-1}).

In our own spectra there is no unequivocal evidence of an absorption feature due solely to monomeric NO. However, the sharp

nature of the 1845 cm^{-1} peak from the unannealed solid in Figure 5 closely resembles that obtained by Smith and Guillory (1977) (cf. Figure 9). In addition, there seems to be another smaller, incompletely resolved absorption located at the base of this peak in Figure 5. Thus, it seems probable that this peak includes contributions from both the NO monomer and the cis-$(NO)_2$ dimer (e.g., the 1866 and 1861 cm^{-1} peaks observed by Smith and Guillory (1977); cf. Figure 9). The relative intensities of these two features seem to interchange under other conditions (e.g., see Figures 6 and 7). Thus, the two major peaks observed for pure NO are most probably due to both the cis-$(NO)_2$ dimer (i.e., at 1845 and 1740 cm^{-1}) and the NO monomer (1845 cm^{-1}), with varying contributions to the higher frequency absorption.

As stated by Lucas (1977), "Experience has shown that every matrix study of one of the oxides of nitrogen tends to become a study of all the oxides of nitrogen." This statement is, of course, also applicable in the current work. In addition to absorption peaks attributed to NO, there are also weaker features present that arise primarily from NO_2 and N_2O contaminants. These become more evident under other conditions; e.g., with larger samples, as in Figure 6, or under conditions where most of the nitric oxide has evaporated, as in Figure 7. In Figure 6, the absorption peak at 2200 cm^{-1} and the composite peak at about 1280 cm^{-1} are attributed to the fundamental stretching modes, ν_3 and ν_1, of N_2O (see section 3.1-1.1 above). Also evident in Figure 6 is a moderately strong unassigned absorption at approximately 3525 cm^{-1} that appears related to N_2O. This absorption is quite evident in the pure N_2O spectrum (shifted to

about 3450 cm^{-1}) presented in Figure 2. It does not appear to be related to either NO or NO_2, since there are no other discernible features due to these two species in Figure 2. In addition, the 3525 cm^{-1} absorption disappears at about 100K upon the desorption of N_2O. Its behavior also appears to be different from that of the broad condensed water absorption at 3200 cm^{-1}, since it appears immediately upon deposition of N_2O, and remains relatively unchanged after one hour, whereas the condensed water absorption continues to increase monotonically with time as water vapor deposition from the background continues.

The absorption peak at about 1585 cm^{-1} in Figure 6 is attributed to monomeric NO_2. Smith and Guillory (1977) assigned a 1612 cm^{-1} absorption to NO_2, as determined directly from NO_2/O_2 films. A 1617 cm^{-1} absorption was assigned to NO_2 (ν_3 stretch) in solid N_2, and 1610 cm^{-1} in solid Ar. It seems reasonable to expect that this absorption would shift to lower frequency in an NO matrix. The same NO_2 peak is also evident in Figure 7 which is a spectrum of the residual from an NO sample at 95K. Also present in the same spectrum is a strong absorption at about 1285 cm^{-1}. However, by 95K all the NO had already desorbed (N.B.P. - 151.8 °C), and although some residual N_2O might still have been present (N.B.P. -88.5 °C), the complete absence of the 2200 cm^{-1} peak (e.g., see Figure 2) argues against this. Thus, some other species must be responsible for the absorption peaks observed in Figure 7.

Since the monomeric NO_2 feature is quite evident in Figure 7, it is reasonable to conclude that the other major features are

probably due to N_2O_4. Smith and Guillory (1977) reported a group of absorption peaks, including 1828, 1644, and 1290 cm^{-1}, that appeared immediately upon warming NO/O_2 solid films. In their work, these features became the most prominent in the spectrum after the O_2 oxidation of NO was complete. Some additional work with NO_2/O_2 films showed that at a high deposition rate these features were the only ones observed in addition to that for NO_2. In well-annealed films, these features disappeared and were replaced by others (attributed to D_{2h}-N_2O_4). Thus, these peaks were assigned to iso-N_2O_4. The well-annealed NO_2/O_2 films were also observed to exhibit features at 1766, 1738, 1279, and 1265 cm^{-1} that were observed to grow steadily during the experiments. These features were assigned to the D_{2h}-N_2O_4 isomer, which is the stable form in the gas phase. Since the iso-N_2O_4 thermally isomerizes into D_{2h}-N_2O_4, this accounts for the continuous growth observed for the absorption features of the more stable isomer. Schaffert (1933) assigned absorption features at 1754 (ν_3) and 1274 (ν_1) cm^{-1} to N_2O_4 in the gas phase. These assignments correspond well to the doublets given by Smith and Guillory (1977) for D_{2h}-N_2O_4; i.e., 1766 and 1738 correspond to Schaffert's 1764 cm^{-1} feature, while 1279 and 1265 correspond to Schaffert's 1274 cm^{-1} feature.

Therefore, concerning Figure 7, the 1850, 1675 (multiplet), and the 1285 cm^{-1} peaks are assigned to iso-N_2O_4, while the 1750 (minor), 1725, and 1250 cm^{-1} peaks are assigned to D_{2h}-N_2O_4.

3.1-1.3. Oxygen and Ozone.

Representative spectra of pure oxygen and oxygen/ozone mixtures are presented in Figures 10 and 11, respectively.

Comparison of these two figures indicates that the absorption features at 1020 and 2080 cm^{-1} are attributable to O_3. These features are close to 1044 (ν_3) and 2125 ($\nu_1 + \nu_3$) cm^{-1} observed by Lucas (1977) for O_3 in a solid nitrogen matrix. Absorptions in solid Ar were observed at 1105 (ν_1), 704 (ν_2), and 1040 (ν_3) cm^{-1}.

All the ozone in the current studies was deposited as 2.5 mol % O_3 in O_2 mixtures. The resultant samples could be concentrated in ozone by allowing the O_3/O_2 mixture to impinge on the sample disk at elevated temperatures. Since the normal boiling point of ozone is greater than that of oxygen (-111.9 °C for O_3 and -183. °C for O_2), ozone can be differentially concentrated in the sample in this manner. An example of this procedure is shown by the spectra in Figure 12 (taken with CdTe transmission windows) where the ozone absorption at 1020 cm^{-1} becomes progressively more intense as O_3 condenses and concentrates at 40K.

3.2. Condensed NO Behavior With Temperature.

One objective of the current work was to observe changes in condensed samples as a function of temperature. In Figure 13, spectra of a pure NO sample are presented as a function of temperature. Some definite qualitative behavior is readily apparent from this figure. Increasing the temperature from 19K to 35K and holding at the latter temperature for approximately five minutes caused the 1745 cm^{-1} feature to grow and become larger than the 1845 cm^{-1} absorption. After thirty minutes, and then one hour at 35K, the situation appeared to remain relatively unchanged. Increasing the temperature to 50K, however, resulted

in a definite increase in intensity of the high frequency feature with respect to the lower one. In order to investigate this behavior further, the spectrophotometer was set on the higher frequency absorption while the temperature was gradually varied. The results of this experiment are presented in Figure 14. As can be seen, the absorption intensity increased continuously from 35K to approximately 50K, whereupon it remained constant to about 63K, at which point it began to decrease quite rapidly.

This preceding behavior is consistent with the results of Smith and Guillory (1977) and our own previous work (Calo et al., 1981, 1982). Smith and Guillory (1977) found that annealing an NO/O_2 sample by increasing the temperature to 35K and then recooling, resulted in a significant increase in the intensity of the absorption features at 1773 and 1861 cm^{-1} ascribed to the cis-$(NO)_2$ dimer. In Figure 14, increasing absorption is apparently due to dimer growth between 35K and 50K that appears to cease at the latter temperature. The rapid decrease beginning at 63K is due to thermal desorption of the sample. In our mass spectrometric work (Calo et al., 1981; cf. Figure 15), thermal desorption of NO clearly exhibited two desorption peaks at 64K and 82K. The first peak coincides almost exactly with the intensity decrease evident in Figure 14. The second peak, however, was not reflected in the IR data. This is explained by the fact that the thermal desorption data are differential in nature, whereas the IR data are integral; i.e., relatively little sample remains to provide strong absorption at 82K where the second desorption peak was observed.

3.3. $NO/O_3/O_2$ Mixtures.

3.3-1. NO Oxidation in the Solid State - Literature.

The solid state analogs of the well-known gas phase reactions:

$$NO + NO + O_2 \longrightarrow 2NO_2 \qquad [R1]$$

and

$$NO + O_3 \longrightarrow NO_2 + O_2 \qquad [R2]$$

have been previously reported in the literature. Lucas (1977) and Lucas and Pimentel (1979) studied $NO/O_3/N_2$ mixtures (typically 1/30/250) on a 12K CsI window, and attributed the growth of the $1617\ cm^{-1}$ band to reaction [R2]. However, even though absorption by the NO_2 product was clearly evident, the high dilution ratios employed resulted in barely discernible changes in the reactant concentrations. The $NO-O_3$ complex was hypothesized as the reaction intermediate, and the reaction rate data were found to be first order with respect to the concentration of the complex, with an apparent rate constant:

$$k_{O3} = 9.9 \times 10^{-4} \exp(-106/RT),\ s^{-1} \qquad (1)$$

The activation energy of 106 cal/g mol is on the order of that required for orientation rearrangement in rare gas matrices, and more than an order of magnitude less than the 2.3 kcal/g mol reported for the gas phase version of reaction [R2]. It was, therefore, hypothesized that matrix rearrangement could be the rate-determining step, although the reason why the reaction should proceed without any activation energy once the reactants are properly oriented was not resolved.

Smith and Guillory (1977, 1977a) observed the overall reaction [R1] for NO in solid oxygen matrices. These workers were able to directly resolve and observe the kinetic mechanism in two distinct steps:

$$NO + NO \longrightarrow cis\text{-}(NO)_2 \qquad [R1\text{-}a]$$

$$cis\text{-}(NO)_2 + O_2 \longrightarrow iso\text{-}N_2O_4 \qquad [R1\text{-}b]$$

Actually, the details of the mechanism include an initial formation of the more stable D_{2h} $-N_2O_4$, followed by a very rapid "uphill" isomerization to the more unstable iso- form (Smith and Guillory, 1977a). It was also stated that this mechanism appears to be the equivalent of the corresponding gas phase reaction, but that in the solid, cage effects do not allow the two product molecules to separate.

Decomposition of the $cis\text{-}(NO)_2$ dimer was found to follow first order kinetics with a rate constant:

$$k_{O2} = 4.25 \times 10^{-2} \exp(-105/RT), \ s^{-1} \qquad (2)$$

Since the observed activation energy of 105 cal/g mol is virtually the same as that for oxidation by ozone in the work of Lucas and Pimentel (1979), it is possible that orientation constraints are rate-determining. More accurately, tunneling was hypothesized to account for the observed isotope effect at 13K, while the orientational requirement was invoked to account for the extremely low frequency factor observed.

3.3-2. Current Observations.

The infrared spectrum presented in Figure 16 was taken immediately following deposition of NO on an O_3/O_2 substrate layer. The two absorption features indicative of NO are clearly evident at about 1845 and 1740 cm^{-1}. Unlike the pure NO spectrum presented in Figure 5, however, both features are significantly broader (especially the higher frequency peak), and (more obviously) the relative intensities of the two peaks are reversed. Also clearly evident are very strong absorption features indicative of NO_2 at about 1570 cm^{-1}, iso-N_2O_4 at 1850 (superimposed on $NO/(NO)_2$ absorption), 1675 (shoulder), and 1285 cm^{-1}, and D_{2h}-N_2O_4 at 1750 and 1725 (superimposed on $(NO)_2$ absorption) and 1250 cm^{-1}.

Obviously, the spectrum in Figure 16 exhibits the results of a large and rapid oxidation of NO by both O_3 and O_2. Since the primary product of the O_3 oxidation reaction in the solid state is iso-N_2O_4 (a la Smith and Guillory, 1977a), the large amount of NO_2 evident in Figure 16 may be the result of direct O_3 oxidation (a la Lucas, 1977, and Lucas and Pimentel, 1979). However, significant amounts of N_2O_4 are also evident, implying that either the O_2 oxidation mechanism was also operative and/or some of the NO_2 formed by O_3 oxidation subsequently dimerized to N_2O_4. In any event, the oxidation reactions had to have occurred relatively rapidly in order to produce such immediate and intense product features. The half-life of NO due to the O_2 reaction mechanism, according to the data of Smith and Guillory (1977a) is about 1.6 min. This time scale is consistent with our experimental observations. The half-life of NO due to the O_3

reaction mechanism, however, (according to Lucas and Pimentel, 1979) is about a factor of 43 greater, or approximately 1.2 hours. This latter time scale is less relevant to the experiment represented by Figure 16. However, due to the layered deposition mode of the experiment, a large amount of NO-O_3 complex could have been formed at the NO-O_2/O_3 interface, resulting in a significant contribution to the product concentration within the time scale of the experiment. Thus, both mechanisms probably contribute significantly to the NO_2 peak in Figure 16.

Several changes occur upon warming of the sample represented in Figure 16. These become evident upon comparison of the spectra in Figures 16 (29K) and 17 (70K):

(1) The 1845 cm^{-1} absorption steadily increases, and the shoulder at about 1810 cm^{-1} in Figure 16 gradually disappears. This is interpreted as indicating the gradual disappearance of NO and cis-$(NO)_2$ due to reaction and desorption, and appearance of iso-N_2O_4 product due to reaction.

(2) The 1740 cm^{-1} absorption steadily decreases, indicative of cis-$(NO)_2$ dimer depletion.

(3) The monomeric NO_2 absorption at 1570 cm^{-1} steadily increases.

(4) The D_{2h}-N_2O_4 features at ~1750, 1725, and 1250 cm^{-1} increase markedly.

(5) The iso-N_2O_4 features at 1850, 1675, and 1285 cm^{-1} increase markedly.

(6) The ozone absorption at 1020 cm^{-1} decreases steadily.

All the preceding observations are indicative of a significant

oxidation of NO to NO_2/N_2O_4 in the solid sample during warm-up.

3.4. Cryogenic Immersion Studies.

3.4-1. Initial Experiments.

Under experimental conditions similar to those used here in previous work (Calo et al., 1981, 1982) high levels of NO_2 were detected with the NO_x chemiluminescence analyzer upon complete rapid desorption of NO_2 samples with ambient temperature nitrogen. But in Figures 5 and 13 the NO_2 absorption peak at 1585 cm^{-1} is notably absent, and it only appears for very large NO samples, as in Figure 6. More notably, however, it does not appear in Figure 13 as the temperature of the NO sample is increased to desorption. Thus, no NO self-disproportionation, according to the stoichiometry,

$$4NO \text{ ---> } 2NO_2 + N_2 \qquad [R3]$$

(see Calo et al., 1981, 1982) is evident from the IR spectra, although it is readily apparent from thermal desorption mass spectrometry and NO_x chemiluminescence. In an attempt to resolve this apparent discrepancy, it was decided to examine some NO samples gas chromatographically before and after freezing out on the walls of a glass vial by immersion in liquid helium.

A 125 ml gas sampling bulb was filed to 2 psig with NO from the gas cylinder (Linde, 98.5 % minimum purity). A sample of this gas, run in a Perkin-Elmer Sigma 3B gas chromatograph with a carbosphere column (6' x 1/8" O.D. teflon tubing packed with 100/120 mesh carbosphere) at room temperature (i.e., oven, injection port, and thermal conductivity detector), yielded a weight ratio of NO_2/NO=0.065 (0.044 molar ratio). In order to

obtain a positive identification of the resultant GC peaks, 50 cm^3 of oxygen was added to the 125 ml gas sampling bulb at 2 psig. An immediate exothermic reaction occurred, resulting in the appearance of the familiar brownish color of NO_2 gas, and a concomitant pressure reduction of about -2.2 psig. Obviously, the well-known reaction, [R1], had occurred. Subsequent GC analysis revealed that the NO_2/NO weight ratio had increased to 1.88. These preliminary tests substantiated that the GC was performing as expected.

In the helium immersion experiment, a 40 ml amber glass vial with a screw cap septum (teflon/silicone) was filled to approximately 5.8 psig with NO. GC spectra were taken before and after immersion in liquid helium (for five minutes). No difference was observed in the NO_2/NO ratio before and after immmersion. This result was puzzling at the time since all other indications were that considerable conversion should have been evident. Subsequent immersion studies followed by gas chromatographic (Poropak T column, 10' x 2mm) analyses yielded similar results, although the chemiluminescence analyzer consistently indicated significant NO self-disproportionation upon thermal desorption from the CdTe IR sample window. In addition, visual observations of color changes in solid NO samples subsequent to cryogenic immersion (see section 3.4-2.) supported the observation that NO self-disproportionation does indeed occur as a result of the condensation cycle.

The visual observation experiments (see section 3.4-2.) also finally helped resolve the discrepancy of the lack of NO_2

detection in the evaporated sample. After warm-up of the condensed NO samples, it was noted that the brownish color of NO_2 gas resulting from NO self-disproportionation showed a marked gradation with vertical position in the gas sample apparatus (cf. Figure 18), with NO_2 concentrating preferentially in the lower dip tube and NO in the upper sample bulb. This was not the result of the slight molecular weight difference per se, but rather as a result of fractionation of the solid sample as it evaporated. Upon removing the dip tube with the condensed sample from the liquid cryogen, NO desorbed first as the sample warmed, filling both the lower dip tube and the upper gas sample bulb. The more condensable NO_2 desorbed at a time considerably later than the bulk of the NO, and concentrated in the lower dip tube where the entire condensed sample originally resided. Thus, all the gas samples drawn off from the upper bulb for gas analysis were concentrated in NO and did not reflect the true extent of volumetric conversion to NO_2.

3.4-2. Visual Observations.

In order to investigate the condensed phase NO self-disproportionation and O_2 oxidation reactions further, some experiments were performed in which NO and NO/O_2 samples were immersed in liquid nitrogen and liquid helium, and the resultant condensed samples were allowed to warm while under visual observation.

The basic apparatus for these studies is shown in the photograph in Figure 18. The gas samples were initially charged to the larger upper sampling bulb. The sample was then evacuated

into the lower, smaller dip tube (immersed in the liquid cryogen) by opening the interconnecting stopcock. In order to more clearly explain the subsequent thermal desorption behavior of the condensed samples, color photographs are used to supplement the written description.

3.4-2.1. NO Experiments.

Pure NO, direct from its cylinder, was admitted to the upper, larger sample bulb shown in Figure 18, to 3 psig at 20 °C. This gas was found to have an NO/NO_x ratio of 0.988 by NO chemiluminescence, and 0.985 by gas chromatography (Poropak T column). Thus, initially, the sample was no greater than 1.5% NO_2 (i.e., if all the NO except NO was NO_2). The still empty dip tube was immersed in a dewar of LN_2 for a few minutes before the stopcock between the sample bulb and the dip tube was opened to evacuate the sample bulb. After a few seconds, the LN_2 dewar was removed, and the dip tube was observed and photographed as the condensed samples warmed. The photographs in Figure 19 show the sequence of events. Figure 19(a) shows the appearance of the dip tube immediately after removal of the LN_2 dewar. The walls are frosted over, and a greenish-yellow liquid is clearly evident at the bottom of the tube. Immediately upon condensation, this liquid is straw-yellow in color, but acquires a more marked greenish tinge as the sample warms. As the liquid evaporates, the tube fills rapidly with gaseous NO since it has a much lower boiling point than NO_2 (NO: N.B.P.= -151.74 °C, M.P.= -163.51 °C; NO_2: N.B.P.= 21.2 °C, M.P.= -11.2 °C), while the liquid at the bottom becomes more greenish (see Figure 19(b)). In Figure

19(c), a distinct blue ring can be observed at the top of the liquid. After most of the sample has evaporated, the remaining liquid is deep blue, and after complete evaporation, the final gas phase has a marked brownish tinge indicative of NO_2. Since this color was not in evidence in the original gas, and since care was taken to insure that no other oxidants were admitted during the process described, the NO must have self-disproportionated to a significant extent. This result is totally consistent with our thermal desorption studies from the cryogenic refrigerator IR sample window.

It is known (Chilton, 1968) that nitrogen peroxide (i.e., the equilibrium mixture of NO_2 and N_2O_4) is yellow in color, and that dinitrogen trioxide, N_2O_3, forms a liquid with a deep blue color. Thus the explanation for the observations reported above seems to be that enough NO_2 is present initially, and/or formed very rapidly, to give the initial resultant liquid its yellow color, but that as the tube warms, NO progressively reacts with nitrogen peroxide to form dinitrogen trioxide, giving the liquid a progressively greener tinge. The blue ring above the greenish-yellow liquid in Figure 19(c) can be explained by the gas phase reaction of NO and NO_2 above the liquid to form dinitrogen trioxide which condenses on the walls at a point that is still below the ~-40 °C required to condense the compound. In the vapor phase, N_2O_3 dissociates extensively to NO and NO_2; in fact, the vapor above liquid dinitrogen trioxide consists of almost pure NO (Chilton, 1968). The final gas mixture is probably almost all NO and NO_2, from which the brownish color of the final gas mixture derives.

3.4-2.2. NO/O_2 Experiments.

Other experiments were conducted to observe the effect of condensed O_2 on NO. In these experiments, after complete evacuation of the sample bulb, pure oxygen was admitted to a pressure of -15 in. Hg. With the dip tube immersed in LN_2, the stopcock was opened, thereby completely transferring the oxygen sample to the dip tube. After closing the stopcock, the sample tube was flushed with helium and evacuated once again. Pure NO, directly from the gas cylinder, was charged to the sample bulb to 3 psig at 20 °C. And, once again, with the dip tube immersed, the NO sample was completely transferred to the dip tube by opening the stopcock. The resultant sample was thus approximately 70.6% NO and 29.4% O_2. After a few seconds, the LN_2 dewar was removed and the changes in the sample observed. Figure 20(a) shows the appearance of the dip tube immediately after removing the dewar. The resultant frost is obviously multicolored. Initially, there are definite layers of blue, green, and yellow. As the frost melts (Figure 20(b) and 20(c)), oranges, reds, and violets appear. After these transient species disappear, only blue liquid droplets, indicative of dinitrogen trioxide, remain (Figure 20(d)). These blue liquid droplets are also quite evident in Figures 20(b,c), As previously, due to its lower melting point, the NO desorbs first, leaving the blue liquid NO_2 condensate behind. The oranges, reds, and violets in Figures 20(a,b,c) are evidently transient intermediates involved in the oxidation of NO. Figure 20(e) shows the appearance of the sample after most of the it has evaporated. The brownish color of NO_2 gas is clearly

evident, as well as a dark blue pool of liquid N_2O_3 at the bottom. In Figure 20(f), taken after the entire sample had evaporated, only the dark brownish color of NO_2 remains.

3.4-2.3. Liquid Helium Experiments.

Due to the temperature limitation imposed by the use of LN_2, both NO and O_2 were actually condensed in the liquid, rather than the solid state. In order to assess whether any differences in behavior could be attributed to this fact, some experiments, similar to the preceding, were performed with liquid helium (LHe). The results of these experiments were qualitatively similar. For initially colorless pure NO samples, the condensation/evaporation process produced a gas sample with a definite brownish color, thereby, once again, substantiating NO self-disproportionation. The qualitative observations for NO/O_2 samples were also similar, except that rapid and heavy frost deposition on the outside of the dip tube made clear observations quite difficult.

3.4-3. Experiments With H_2O.

In addition to the preceding experiments, the effect of water on NO conversion was also investigated. In one such experiment, 10 cm^3 of oxygen was added to an NO gas sample with an NO_2/NO weight ratio of 0.16, at atmospheric pressure. As expected, the NO_2/NO ratio increased to 0.845. To this mixture was added 1 ml of liquid distilled water. The NO_2/NO ratio increased further to 1.84. In order to determine whether dissolved oxygen in the water might have been responsible for the

additional conversion, the sample vial was charged with a small amount of liquid water which was then pumped off until all the visible liquid evaporated and about 100 μm of water vapor remained. NO sample gas was then charged to the vial to a total pressure of one atmosphere. Once again, the results were similar; i.e., the final NO_2/NO weight ratio was arout 2.125, thereby indicating a large conversion of NO to NO_2 due to water. [Since both oxyacids of nitrogen require NO_2 for formation with water (see section 3.5, reactions [R4] and [R5]), enough NO_2 must have been present initially to initiate the conversion process. Once formed, the acids readily decompose, since at room temperature the equilibrium constants for formation of the acids are relatively low. This yields more NO_2 (reaction [R5]) which can then further react with excess water to produce additional acid, etc. Thus, in this manner the acids can "catalytically" oxidize NO.]

These experiments indicated that the water-related aspects of interconversion among the oxides of nitrogen could be a central issue in understanding the behavior of NO_x in cryogenic whole air samples. Further investigations concerning this facet are reported in the next section.

3.5. The Role of H_2O in NO Self-Disproportionation and Oxidation.

The chemistry of water and the oxides of nitrogen is quite important both from an atmospheric viewpoint and commercially in the manufacture of nitric acid. The two oxyacids of most interest here are nitrous acid, HNO_2, and nitric acid, HNO_3. Both of these species are known to occur in the stratosphere and are important

participants in the H-NO_x cycle (e.g. see "The Stratosphere 1981...," 1982), as well as in the currently popularized issues related to acid rain. Since water is a relatively abundant minor stratospheric constituent (~3 ppm), it is definitely present in whole air samples. Due to its intimate involvement in NO_x chemistry its effect on the solid sample and subsequently upon desorption, is of considerable interest. In view of this situation, the following experiments were conducted in order to define the effect of H_2O on NO conversion.

3.5-1. NO Self-Disproportionation in the Presence of H_2O.

It was previously noted that in Figures 5 and 13 the NO_2 absorption peak, as well as all the N_2O_4 features, were notably absent from the IR spectra even upon warming to desorption. However, as the cryogenic immersion studies in the previous section, and mass spectrometric and chemiluminescence studies have shown (see Calo et al., 1981), NO does self-disproportionate significantly into NO_2 and N_2 a la reaction [R3]. Thus, there must be a plausible explanation for why no absorption due to NO_2 is observed in the IR spectra of Figures 5 and 13.

In both these figures, a significant absorption due to condensed water vapor is quite evident in the omnipresent broad feature at about 3150 cm^{-1}. This condensed water originates primarily from deposition of background water vapor in the refrigerator vacuum shroud. In order to investigate the correlation between the appearance of the NO_2 absorption peak and condensed water vapor, a series of experiments was conducted in which the amount of water vapor was varied. The auxiliary

cryogenic refrigerator was used as a cryopump to minimize the accumulation of water vapor from the background, and additional controlled amounts of water were admitted as described in the experimental procedures outlined in Appendix B. Although it was difficult to accurately determine the total absolute amount of water deposited onto the IR sample window during each experiment, the relative amount of water in excess of the background present with the cryopump in operation was estimated as the difference between the peak absorbance and an arbitrary baseline value equivalent to 90% transmission.

The results of four experiments conducted by deposition of 50 mmol of NO on a substrate of varying amounts of water vapor (i.e., Type I experiment; see section 3.5-2.) are summarized in Table I. The total conversion to NO_x upon thermal desorption for each case was determined using the procedure outlined in Appendix B. Two interesting results are evident upon examination of the data in Table I. First, the intensity of the NO_2 absorption peak is inversely proportional to the amount of water vapor present in the substrate; and second, the total conversion to NO_x remains relatively constant with respect to the total amount of water deposited. In addition, the two absorption peaks indicative of pure NO were observed to become more nearly equal with increasing NO_2 absorption, indicative of increasing iso-N_2O_4 as observed previously (see section 3.3-2.). Thus, in the presence of almost no water (e.g., run 9) the products of NO self-disproportionation are clearly evident in the IR spectra; whereas in the presence of larger amounts of water they are not apparent. However, in all cases the eventual final conversion to NO_x remains approximately

constant.

One explanation for this behavior is that in the presence of significant amounts of water, the NO_2 resulting from self-disproportionation is rapidly converted to the two oxyacids of nitrogen, HNO_2 and HNO_3; however, as explained below, unequivocal proof of this process was not obtained. The basic stoichiometries for the production of the oxyacids are:

$$NO + NO_2 + H_2O \longrightarrow 2HNO_2 \qquad [R4]$$

and

$$3NO_2 + H_2O \longrightarrow 2HNO_3 + NO \qquad [R5]$$

Clearly evident from these reactions is that the statement quoted from Lucas (1977) in section 3.1-1.2, concerning the interrelated nature of the oxides of nitrogen, also readily extends to the oxyacids. As presented by Ashmore and Tyler (1961), for example, the presence of nitrous acid in the vapor phase inevitably results in a mixture of NO, NO_2, NO_3, N_2O_4, HNO_2, HNO_3, and H_2O. The chemical equilibria among the various species are highly coupled, and the thermodynamic properties of the reactions are well-known. Since both reactions [R4] and [R5] are exothermic, their equilibrium constants decrease with increasing temperature. The resultant equilibrium constant for [R4] at 20^{o} C is about 1.56 atm^{-1}, while at 25^{o} C the corresponding equilibrium constant for reaction [R5] is approximately 0.01 atm^{-1}. Thus, formation of both acids is thermodynamically favored under conditions prevalent in the condensed cryogenic samples of interest in the current work, while significant decomposition of the acids is favored in the resultant gas phase from thermal desorption of

these samples that is fed to the chemiluminescence analyzer at ambient temperature. As an example of the latter point, Ashmore and Tyler (1961) give the following vapor phase compositions for reaction mixtures initially consisting of NO_2, NO, and H_2O:

T(°C)	NO_2	N_2O_4	N_2O_3	NO	H_2O	HNO_2	HNO_3
19.95	0.0275	0.0060	0.0142	0.9051	0.0229	0.0243	0.0001
80.7	0.0311	0.0001	0.0008	0.7753	0.1739	0.0187	0.00007

These figures show quite clearly that that acids are not favored in the vapor phase at room temperature and above; especially HNO_3.

There are some serious problems associated with unambiguous identification of IR absorption features attributable to the acids in the presence of large amounts of NO, NO_2, and H_2O. This is, of course, due to the fact that the absorption features of the oxyacids of nitrogen are superimposed on the very strong fundamental O-H, N-O, and N=O frequencies of the reactants. Jones et al (1951) studied the IR spectra of HNO_2 in the vapor phase. It was concluded that HNO_2 exists as two tautomeric forms, cis and trans (with the latter being the more stable, and thus the more prevalent form -- approximately a factor of three greater at room temperature). Absorptions due to: O-H stretch (ν_1) at 3426 (cis) and 3590 (trans); O-H bend (ν_3) at 1260 (trans) and 1292 (cis); O-N stretch (ν_4) at 794 (trans) and 856 (cis); and O=N stretch (ν_2) at 1696 (trans) cm^{-1}, were reported. The IR absorption characteristics of HNO_3 vapor were examined by Cohn et

al. (1952). The followins major features were evident: O-H stretch at 3560; O-H bendins at 1335; and NO_2 stretch at 1320 and 1710 cm^{-1}. Even a cursory examination of these absorptions, allowins for shifts due to the solid matrix, clearly indicates the problem of superposition on initial reactant peaks.

Attempts at positive identification of the acids by sas chromatosraphy, usins both the carbosphere and Poropak T columns, met with problems similar to those for the IR spectra; i.e., acid peaks could not be separated from those of the reactant species. NO_x chemiluminescence, of course, results in the acids showins up as additional NO_x due to thermal decomposition, and thus is also incapable of providins the necessary discrimination. Thus, although a mechanism involvins the formation of the acids in the condensed sample can explain the current observations, direct evidence of their presence was not obtained.

3.5-2. NO Oxidation in the Presence of H_2O.

In order to explore the effects of additional oxidation in the condensed sample due to O_3 and O_2, on the final conversion of NO upon thermal reseneration, a number of experiments were conducted. These were classified accordins to the nature of the sample deposition mode, as set forth in Table II. All of the experiments reported on in this section were performed in accordance with the procedures outlined in Appendix B.

The results of a number of these types of experiments are summarized in Table III. The relative water content in Table III is taken as the difference between the peak absorbance at 3200 cm^{-1}, measured immediately after sample deposition, and the

baseline absorbance corresponding to 90% transmittance. A similar procedure was used to determine the relative NO_2 content using the 1585 cm^{-1} absorption peak. The NO conversions were determined from the post-regeneration gas sample, as measured with the chemiluminescence analyzer, in accordance with the procedure described in Appendix B.

The results regarding total conversion to NO_x as a function of relative water content are summarized in Figure 21. The effect of the additional conversion to NO by oxidation in the condensed state is quite evident. In addition, there is a definite trend in the manner in which the relative water content affects total conversion. As shown in Figure 21, at low relative water content the effect on NO conversion increases rapidly. However, at higher water content the NO conversion approaches a limiting asymptotic value; i.e., after a certain amount of water is present, additional water has no effect. This result can also be explained in terms of an acid intermediate conversion mechanism, as proposed in the preceding section, in terms of the relative amounts of H_2O and NO_2. With NO_2 available in considerable excess due to production in the condensed phase by O_2 (beyond that expected for just self-disproportionation), additional conversion of NO_x can occur via reaction [R4] to produce nitrous acid. However, as the amount of water is increased, a point is reached where the NO_2 availability for acid production becomes limiting, in which case, additional conversion of NO is reduced. Of course, this mechanism implicitly assumes that thermodynamic equilibrium overwhelmingly favors the acid, and that the conversion process,

although perhaps initially rapid at interfacial points of contact, eventually becomes kinetically limited and slow. From the data presented in sections 3.3-1 and 3.5-1, the formation of the acid is indeed thermodynamically favored at low temperature, and as the available amount of NO_2 decreases, the conversion process should also slow significantly. Thus, the situation hypothesized seems likely. This explanation is also consistent with the NO self-disproportionation results presented in section 3.5-1, if the availability of NO_2 is already limiting due to the lower inherent conversions.

The correlation between the NO_2 absorption peak at 1585 cm^{-1} and the overall conversion of NO, however, seems to be less clear. In certain experiment sets in Table III (e.g., Runs 13, 26, and 28; Type VII), the NO_2 peak clearly increases as the water content decreases, exactly as in the NO self-disproportionation experiments (Runs 4, 9, 18, and 24). But in other sets, the NO_2 absorption peak either remained relatively constant (e.g., Runs 15, 22, and 25), or actually decreased slightly (Runs 3, 21, and 31). The detailed behavior of NO_2 in the condensed sample is complicated by the larger production rate due to the oxidants reacting with NO, as well as the competing reaction paths to N_2O_4 and the acids. For example, in Figure 22 (Run 15; Type IV), the features characteristic of large amounts of N_2O_4 are readily apparent (compare Figures 7 and 22). Thus, the behavior of monomeric NO_2 in these types of condensed samples becomes a more complex function of the total and relative amounts of NO, H_2O, and oxidants., than in the self-disproportionation case.

Of all the sample/deposition types, IV exhibited the highest NO conversion by a significant amount (cf. Table III and/or Figure 21). Type IV differs from types II and III due to the 20% more O_2, and also due to the co-deposition of NO and O_2. Admittedly, the enhanced conversion of type IV could be due to the greater interfacial area available for reaction in the condensed phase because of the more homogeneous nature of the sample, and/or some gas phase conversion during the deposition process. However, since co-deposition did not seem to be a very important factor in the type VII experiments (which differ from types V and VI in the same manner as the type IV differ from types II and III), the controlling factor responsible for the bulk of the higher conversions observed in the type IV experiments clearly seems to be the additional O_2. This is also supported by a comparison of the type II/III results (50 mmol O_2) and the type V/VI (58.5 mmol O_2, 1.5 mmol O_3). Furthermore, that gas phase conversion during the deposition process is not significant, is supported by the NO conversions for the type VII (co-deposition) experiments, that are actually slightly less than those for the type V/VI (layered deposition) experiments.

It is also interesting to note that in the layered deposition experiments, the order of deposition seems to make no observable difference (e.g., compare types II/III to types V/VI). This seems to imply that the interfacial area between the NO and O_x layers is the most important factor. This interface remains at the same distance from the H_2O layer no matter whether NO or O_x is deposited first. Thus, the rate of interdiffusion between

oxidized NO and H_2O remains the same during any of the acid formation processes.

The results of the type IV and VII experiments indicate a significantly lower NO conversion efficiency for O_3 in comparison to O_2. Averaging the type VII results yields an NO conversion of 0.6, whereas the value for the type IV results is about 0.7. Thus, for the 2.5% reduction in O_2 from the type VII to the type IV experiments, an apparent 14.3% reduction in NO conversion results. On the basis of just stoichiometry (according to [R1] and [R2]) this reduction in O_2 and replacement by an equal molar amount of O_3 should result in only a 1.25% reduction in NO conversion, if the product O_2 in [R2] is not available to further convert NO according to [R1]. Obviously, then the net effect is not stoichiometrically, but perhaps kinetically limited. This observation is also consistent with the relative magnitudes of the two solid phase rate constants (as given in section 3.3-1), $k_{03}/k_{02} = 2.3 \times 10^{-2}$.

In summary, the results presented in Table III and Figure 21 are consistent with significant oxidation of NO by O_x in the condensed phase, and the enhancement of NO conversion in the presence of condensed water via a mechanism involving the oxyacids of nitrogen.

4.0. CONCLUSIONS.

This report conveys the results of an investigation concerned with the effects of chemical reactions in cryogenically condensed $NO/O_x/H_2O$ samples on the alteration of sample composition upon subsequent thermal desorption. These studies

were undertaken to elucidate the relevant mechanisms and improve the understanding of these processes as they relate to the analysis of cryogenically-collected stratospheric whole air samples acquired in the balloon-borne sampling project of the composition task of the Stratospheric Environment Program of the Air Force Geophysics Laboratory.

The major features of infrared spectra of condensed samples were interpreted in terms of assignments to the various species of interest. Experiments with NO substantiated that condensed NO self-disproportionates to a significant degree upon thermal regeneration. Furthermore, it was found that the intensity of the absorption peak indicative of NO_2 formation in the condensed sample was inversely proportional to the total amount of water in the sample, although the final conversion to NO_x upon thermal desorption remained approximately constant. This behavior was interpreted as an NO conversion mechanism involving the nitrogen oxyacids, nitrous and nitric acids, in the presence of large amounts of water in the condensed sample. This could not be directly proven since the infrared absorption features of the acids are obscured by the N-O and O-H features, and the two gas chromatographic column packings that were tried could not provide unambiguous separation of the acids. However, the fact that water does play a significant role in total NO conversion was shown in experiments including O_2 and O_3 in the condensed sample. In these experiments, the O_3 was observed to convert NO to NO_2 in the condensed sample, which then presumably reacted readily to acids, resulting in significantly increased conversion to NO_x

upon thermal desorption, over and above that measured for NO alone.

In addition to the infrared/NO_x chemiluminescence studies, separate sample immersion studies in liquid nitrogen and helium were conducted which permitted visual observations of the condensed samples upon warming. These studies qualitatively substantiated the other NO conversion results, and were used as an aid in understanding and interpreting the other experiments.

The results of this work indicate that interconversion of the oxides of nitrogen in condensed samples, especially in the presence of water vapor, is a significant process under certain conditions. However, additional work involving careful cryogenic deposition of very small amounts of the various species, combined with perhaps high resolution FTIR, is definitely needed in order to quantitatively assess the relative importance of these same processes in the much more highly dilute stratospheric cryogenic whole air samples.

5.0. REFERENCES.

Arin, L.M. and P. Warneck, J. Chem. Phys., 26, 1514, 1972.

Ashmore, P.G. and B.J. Tyler, J. Chem. Soc. (London) 1017 (1961).

Bellamy, L.J., The Infrared Spectra of Complex Molecules, Wiley, N.Y., 1975.

Calo, J.M., R.J. Fezza,and E.J. Dineen, "Gas-Surface Interactions in Cryogenic Whole Air Sampling," Final Report, Air Force Geophysics Laboratory, Hanscom AFB, MA, AFGL-TR-81-0162, May 1981, ADA108255.

Calo, J.M., R.J. Fezza, and G.F. Ryan, "Chemical Reactions and Molecular Aggregation in Cryogenic Whole Air Sample Matrices," Final Report, Air Force Geophysics Laboratory, Hanscom AFB, MA, AFGL-TR-82-0061, January 1982, ADA114661.

Chilton, T.H., Strong Water. Nitric Acid: Sources. Methods of Manufacture. and Uses, MIT Press, Cambridge, MA, 1968.

Cohn, H., C.K. Ingold, and H.G. Poole, J. Chem. Soc. (London) 4272 (1952).

Dietz, V.R. and J.L. Bitner, Carbon 11, 393 (1973).

Fateley, W.G., H.A. Bent, and B. Crawford, Jr., J. Chem. Phys. 31, 204 (1959).

Gallagher, C.C., C.A. Forsberg, R.V. Pieri, and G.A. Faucher, "Stratospheric Trace Gas Composition Studies Utilizing In Situ Cryogenic Whole-Air Sampling Methods," AFGL-TR-81-0071, Air Force Geophysics Laboratory, Hanscom AFB, MA, 1981, ADA104375.

Guillory, W.A. and C.E. Hunter, J. Chem. Phys. 50, 3516 (1969).

Hallam, H.E., and G.F. Scrimshaw, in Vibrational Spectroscopy of Trapped Species, H.E. Hallam, ed., Wiley, N.Y., 1973, pp. 12-66.

Jenkins, A.C., "Ozone Chemistry and Technology," Adv. Chem. Ser., American Chemical Society, Washington, D.C., 1959.

Jones, L.H., R.M. Badger, and G.E. Moore, J. Chem. Phys. 19, 1599 (1951).

Lucas, D., "Fast Reactions, Free Radicals, and Molecular Complexes Studies by the Matrix Isolation Technique," Ph.D. Thesis, University of California at Berkley, 1977, Univ. Micro. 77-31, 448.

Lucas, D. and G.C. Pimentel, J. Phys. Chem. 83. 2311 (1979).

Marcus, R.A. and J.M. Fresco, J. Chem. Phys. 27, 564 (1957).

Schaffert, R., "The Infrared Absorption Spectra of NO2 and N2O4," J. Chem. Phys. 1, 507 (1933).

Smith, A.L., W.E. Keller, and H.L. Johnston, "The Infrared and Raman Spectra of Condensed Nitric Oxide," J. Chem. Phys. 19, 189 (1951).

Smith, G.R. and W.A. Guillory, "Spectroscopy of the Thermal Oxidation of NO in Solid Oxygen at Cryogenic Temperatures," J. Mol. Spect. 68, 223 (1977a).

Smith, G.R. and W.A. Guillory, Int. J. Chem. Kinetics 9, 953 (1977a).

Snelson, A., "The Chemical Composition of the Atmosphere at 40,000 to 65,000 Feet Using a Modified Matrix Isolation Technique," Project Suggestion IITRI-72-107CX, IIT Research Institute, Chicago, 1972.

Varetti, E.L. and G.C. Pimentel, J. Chem. Phys. 55, 3813 (1971).

"The Stratosphere 1981. Theory and Measurements,"WMO Global Ozone Research and Monitoring Project, Report No. 11, May 1981, NASA/Goddard Space Flisht Center, Greenbelt, MD, January 1982.

Table I.

The effect of water on NO self-disproportionation.

Run #	Relative Amount of Water		Relative Amount of NO_2		NO Conversion to NO x
	$\Delta\%T$ *	ΔA	$\Delta\%T$ *	ΔA	
18	69	0.632	1	0.005	0.364
24	31	0.183	2	0.010	0.361
4	9.5	0.048	5.5	0.027	0.348
9	5	0.025	17.5	0.094	0.383

* 90% transmittance assumed as the baseline.

Table II.

Sample types and deposition modes.

Sample Type	Deposition Mode
I.	NO on H_2O substrate.
II.	NO layer on O_2 layer on H_2O substrate.
III.	O_2 layer on NO layer on H_2O substrate.
IV.	Homogeneous layer of NO and O_2 on H_2O substrate (co-deposition of NO and O_2).
V.	NO layer on O_3/O_2 layer on H_2O substrate.
VI.	O_3/O_2 layer on NO layer on H_2O substrate.
VII.	Homogeneous layer of NO and O_3/O_2 on H_2O substrate (co-deposition of NO and O_3/O_2).

Table III.

The effect of water on NO conversion in NO/O_2 mixtures.

Run #	Deposition Type	NO	O_2 (mmol)	O_3	$\Delta A^*_{H_2O}$	$\Delta A^*_{NO_2}$	NO Conversion to NO_x
18	I	50	-	-	0.632	0.005	0.364
24	I	50	-	-	0.183	0.001	0.353
4	I	50	-	-	0.048	0.027	0.340
9	I	50	-	-	0.025	0.094	0.376
6	II	50	50	-	0.165	0.141	0.551
32	II	50	50	-	0.030	0.046	0.574
31	III	50	50	-	0.539	0.097	0.581
21	III	50	50	-	0.210	0.051	0.573
3	III	50	50	-	0.057	0.065	0.515
22	IV	50	60	-	0.106	0.242	0.739
15	IV	50	60	-	0.040	0.230	0.718
25	IV	50	60	-	0.018	0.234	0.645
33	V	50	58.5	1.5	0.326	0.062	0.703
23	V	50	58.5	1.5	0.025	0.051	0.615
27	VI	50	58.5	1.5	0.097	0.079	0.671
29	VI	50	58.5	1.5	0.062	0.046	0.652
26	VII	50	58.5	1.5	0.122	0.158	0.595
28	VII	50	58.5	1.5	0.079	0.214	0.653
13	VII	50	58.5	1.5	0.010	0.255	0.546

* 90% transmittance assumed as the baseline.

Figure 1. Schematic of the experimental apparatus.

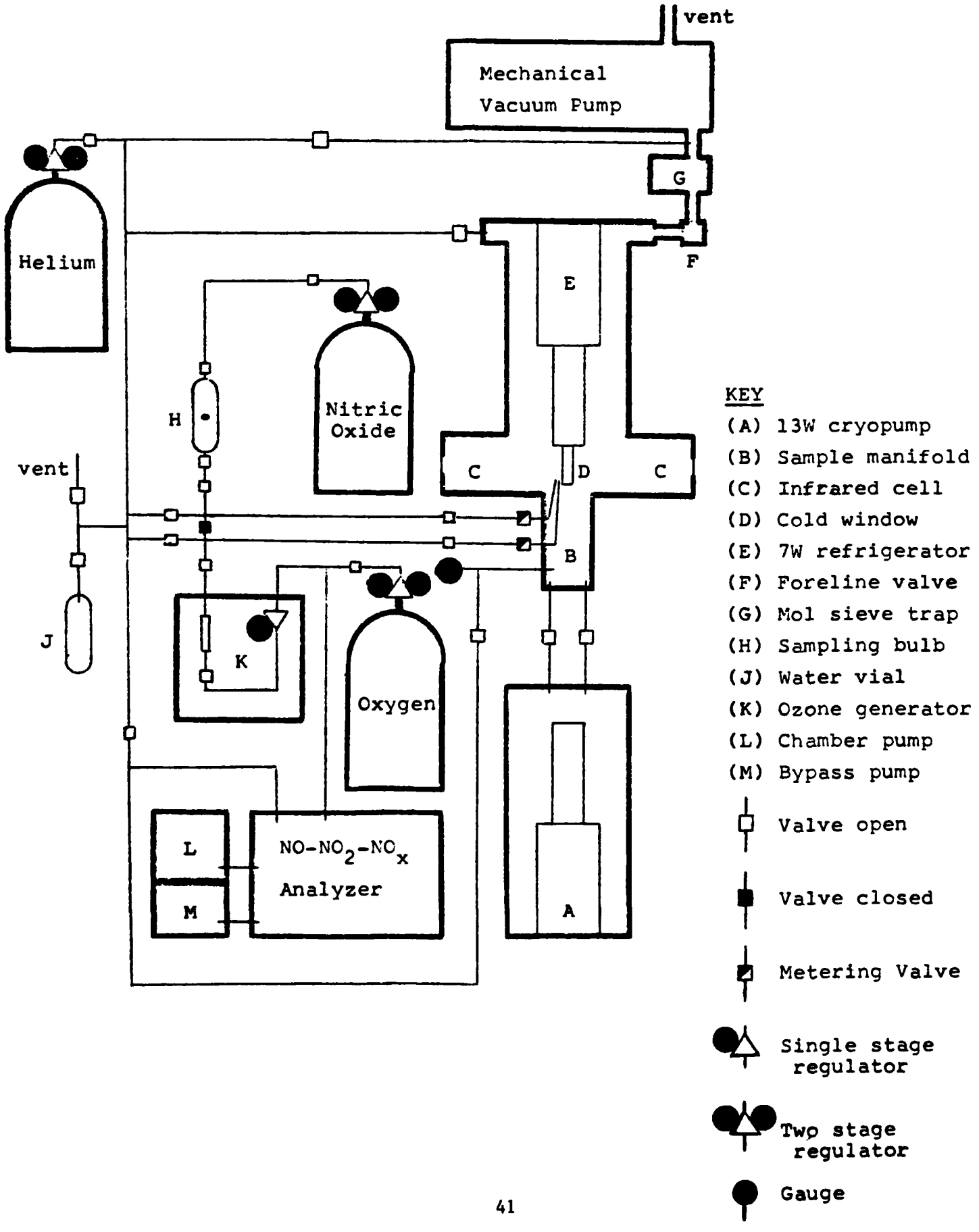
vent
Mechanical
Vacuum Pump
G
Helium
F
E
H
Nitric
Oxide
vent
C
D
C
B
J
K
Oxygen
L
M
NO-NO2-NOx
Analyzer
A
KEY
(A) 13W cryopump
(B) Sample manifold
(C) Infrared cell
(D) Cold window
(E) 7W refrigerator
(F) Foreline valve
(G) Mol sieve trap
(H) Sampling bulb
(J) Water vial
(K) Ozone generator
(L) Chamber pump
(M) Bypass pump
Valve open
Valve closed
Metering Valve
Single stage regulator
Two stage regulator
Gauge

Figure 2. Infrared spectrum of N_2O at 18K (CaF_2 transmission windows).

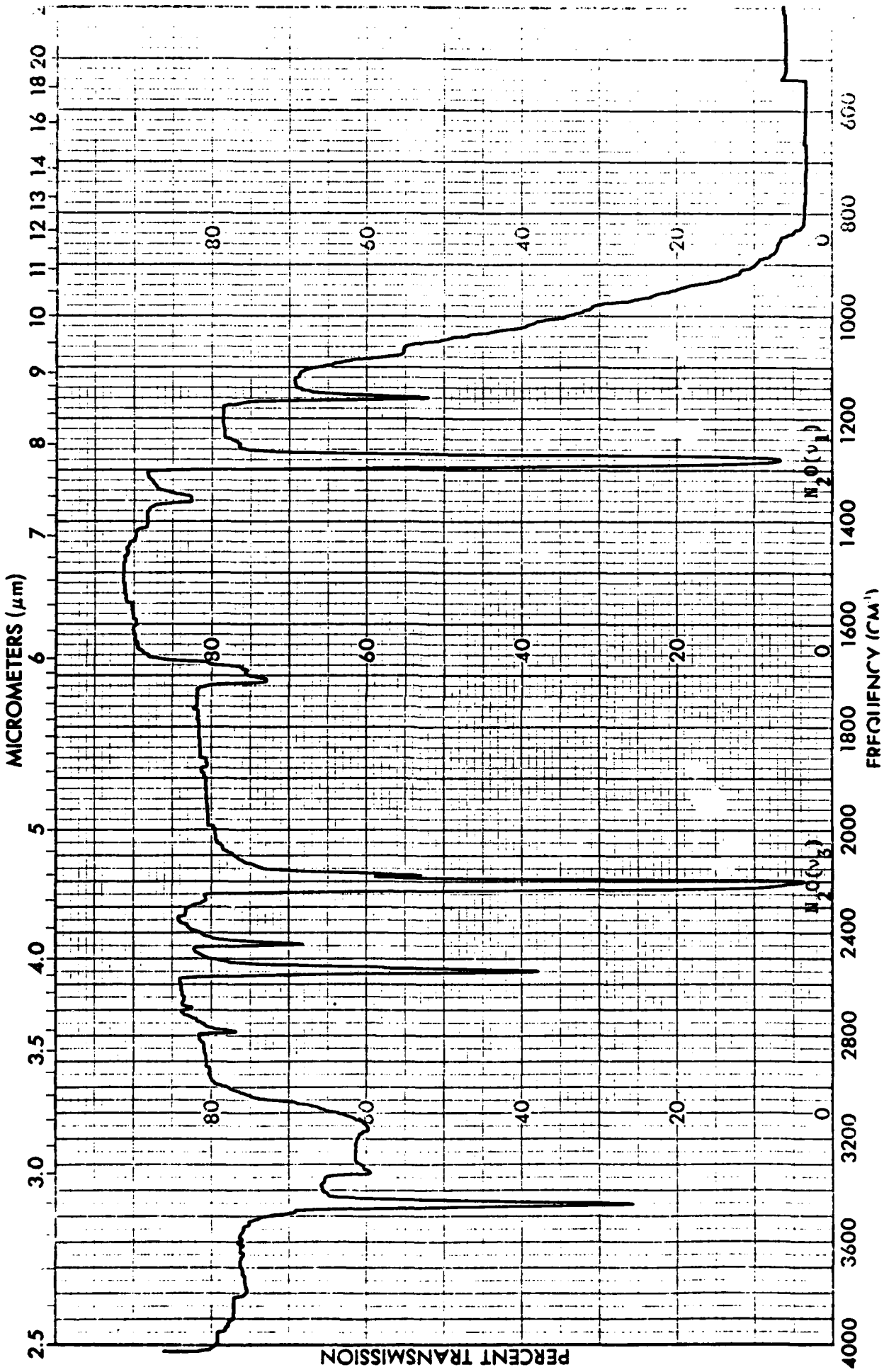
MICROMETERS (μm)
2.5
3.0
3.5
4.0
5
6
7
8
9
10
11
12
13
14
16
18
20
4000
3600
3200
2800
2400
2000
1800
1600
1400
1200
1000
800
660
FREQUENCY (CM⁻¹)
PERCENT TRANSMISSION
0
20
40
60
80
$N_2O(\nu_3)$
$N_2O(\nu_1)$

Figure 3. Variation of condensed N_2O sample spectrum with temperature in the vicinity of 3200 cm^{-1}.

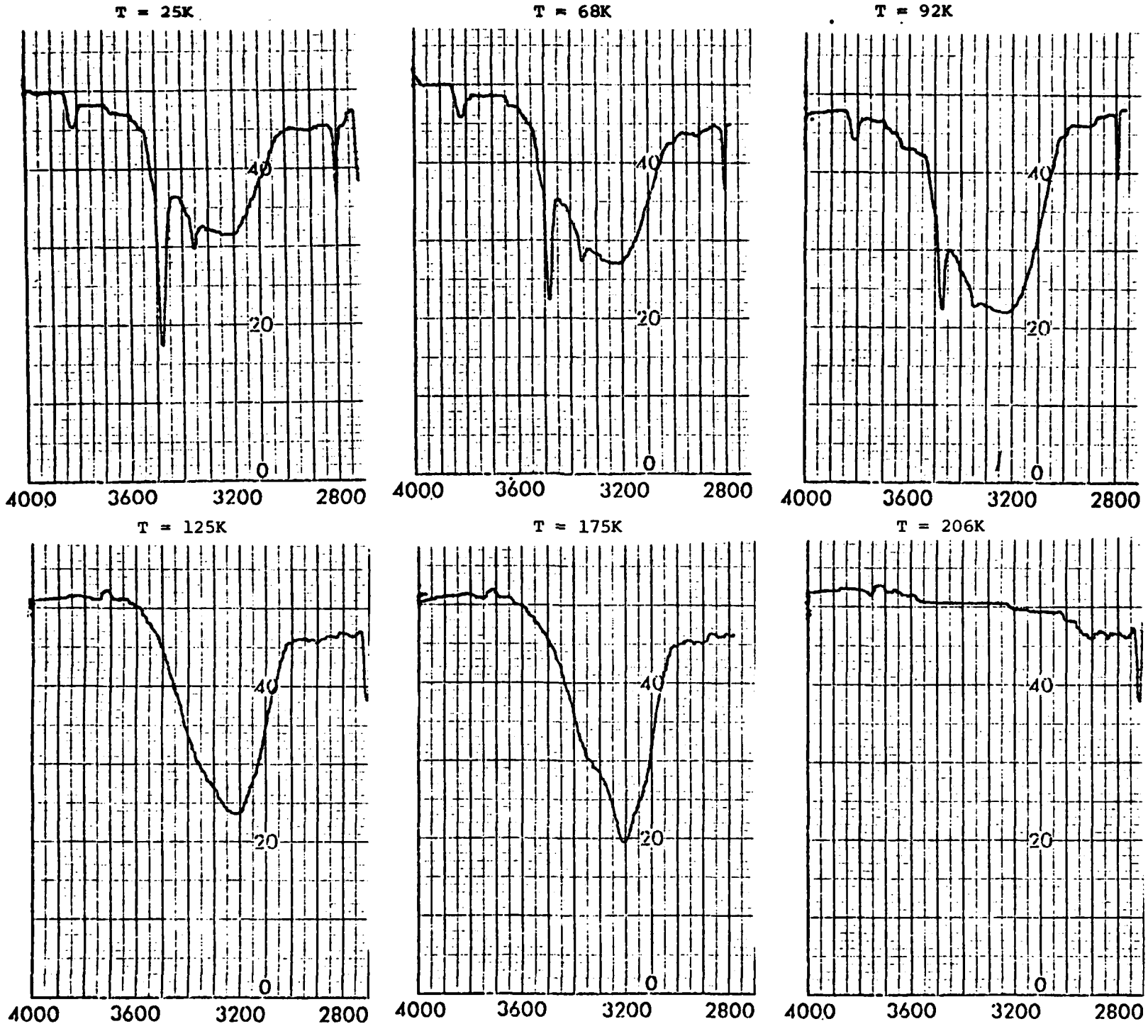
T = 25K
T = 68K
T = 92K
T = 125K
T = 175K
T = 206K
40
20
0
4000
3600
3200
2800
PERCENT TRANSMISSION
FREQUENCY (cm^{-1})

Figure 4. Infrared background spectrum of empty cell at 16 K (CaF_2 transmission windows).

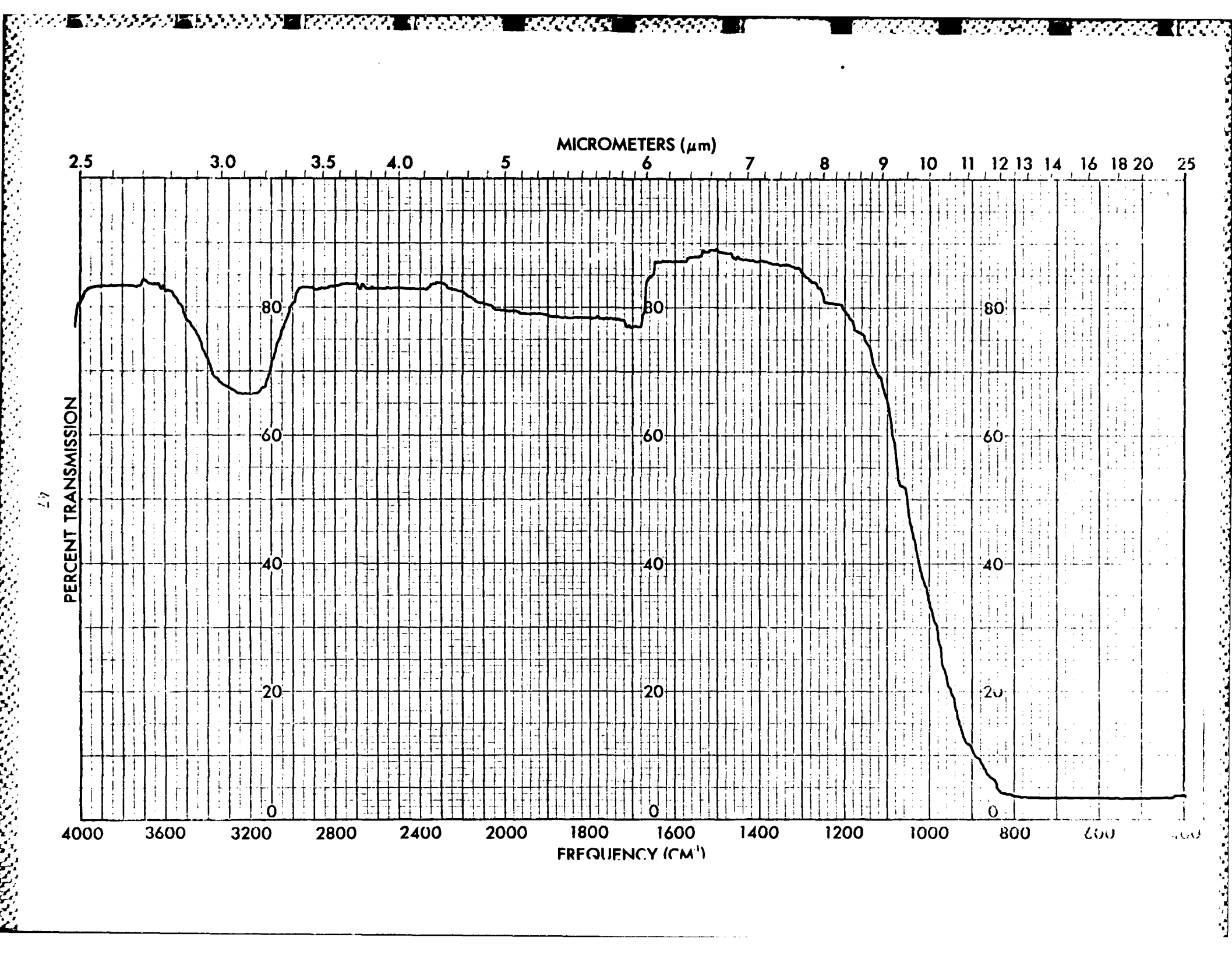
MICROMETERS (μm)
2.5
3.0
3.5
4.0
5
6
7
8
9
10
11
12
13
14
16
18
20
25
PERCENT TRANSMISSION
80
60
40
20
0
4000
3600
3200
2800
2400
2000
1800
1600
1400
1200
1000
800
FREQUENCY (CM⁻¹)

Figure 5. Infrared spectrum of condensed NO at 17 K (CaF_2 transmission windows).

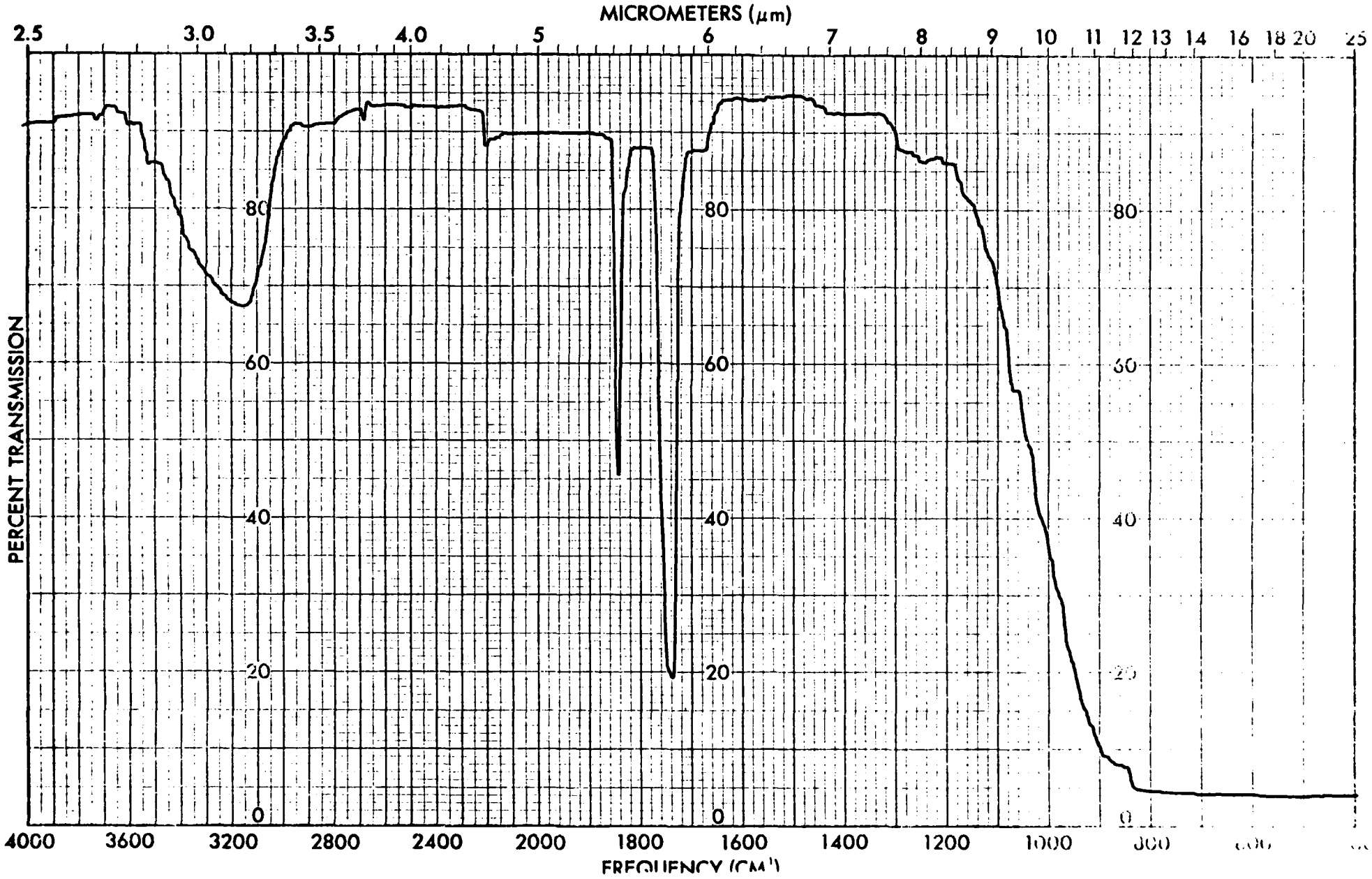
MICROMETERS (μm)
2.5
3.0
3.5
4.0
5
6
7
8
9
10
11
12
13
14
16
18
20
25
PERCENT TRANSMISSION
100
80
60
40
20
0
4000
3600
3200
2800
2400
2000
1800
1600
1400
1200
1000
800
600
FREQUENCY (CM⁻¹)

Figure 6. Infrared spectrum of condensed NO at 18 K for a large sample (CaF_2 transmission windows).

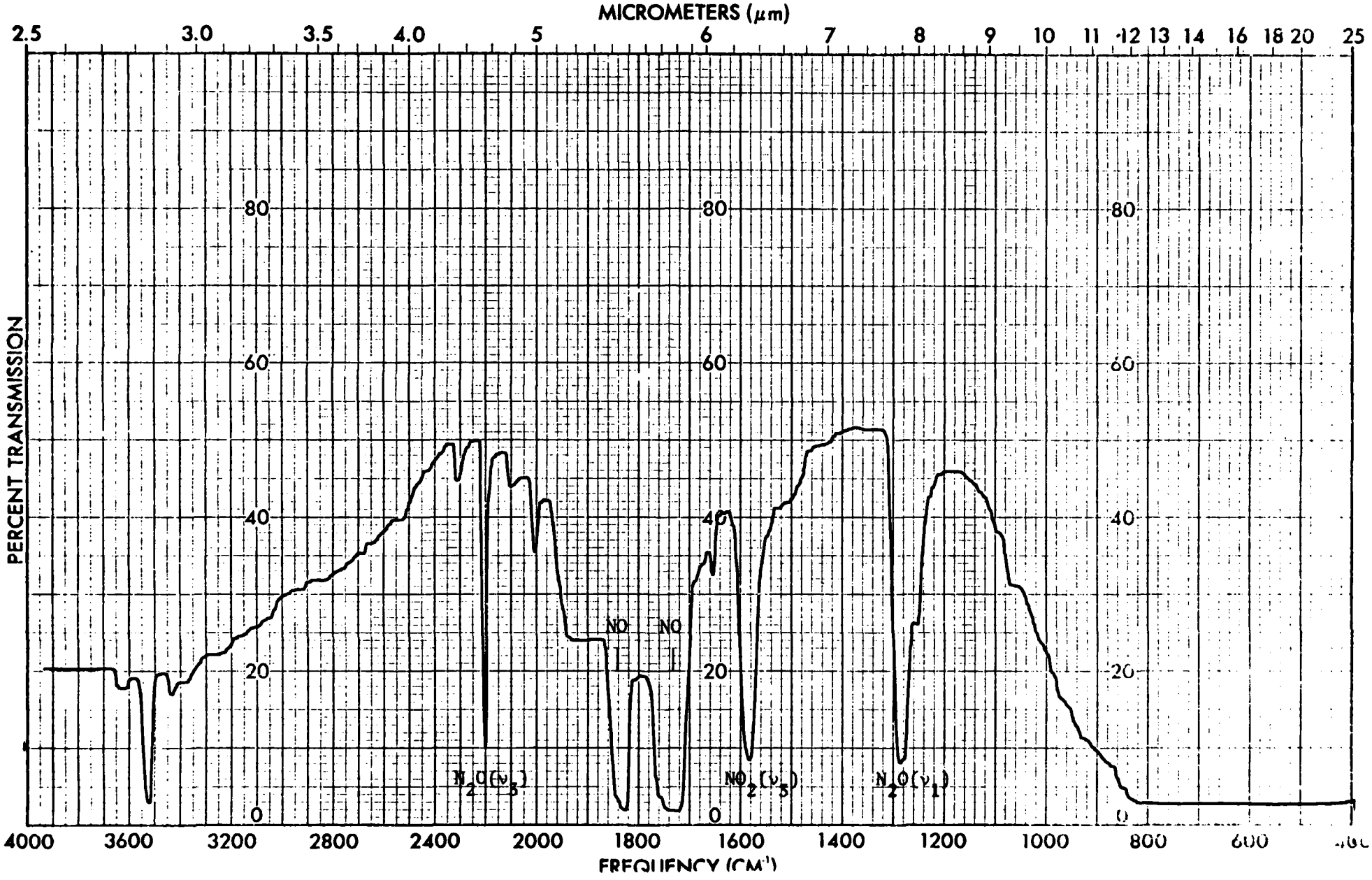
MICROMETERS (μm)
2.5
3.0
3.5
4.0
5
6
7
8
9
10
11
12
13
14
16
18
20
25
PERCENT TRANSMISSION
80
60
40
20
0
NO
NO
$N_2O(\nu_3)$
$NO_2(\nu_3)$
$N_2O(\nu_1)$
4000
3600
3200
2800
2400
2000
1800
1600
1400
1200
1000
800
600
FREQUENCY (CM⁻¹)

Figure 7. Infrared spectrum of residual from a condensed NO sample at 95 K.

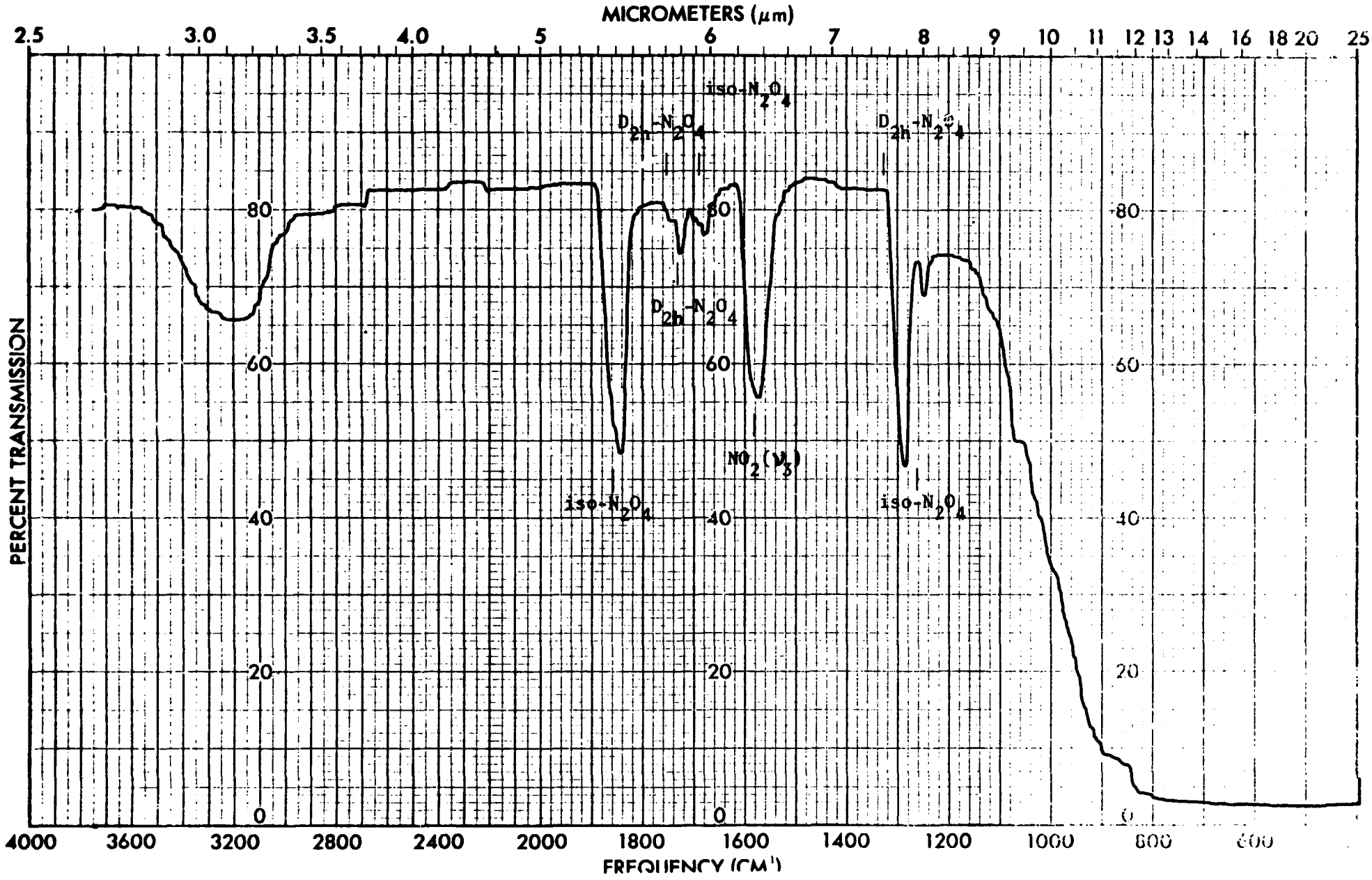
MICROMETERS (μm)
2.5
3.0
3.5
4.0
5
6
7
8
9
10
11
12
13
14
16
18
20
25
PERCENT TRANSMISSION
100
80
60
40
20
0
4000
3600
3200
2800
2400
2000
1800
1600
1400
1200
1000
800
600
FREQUENCY (CM⁻¹)
iso-N2O4
D2h-N2O4
D2h-N2O4
D2h-N2O4
NO2 (ν3)
iso-N2O4
iso-N2O4

Figure 8. Infrared spectra of condensed NO from Smith Keller, and *Johnston* (1951).

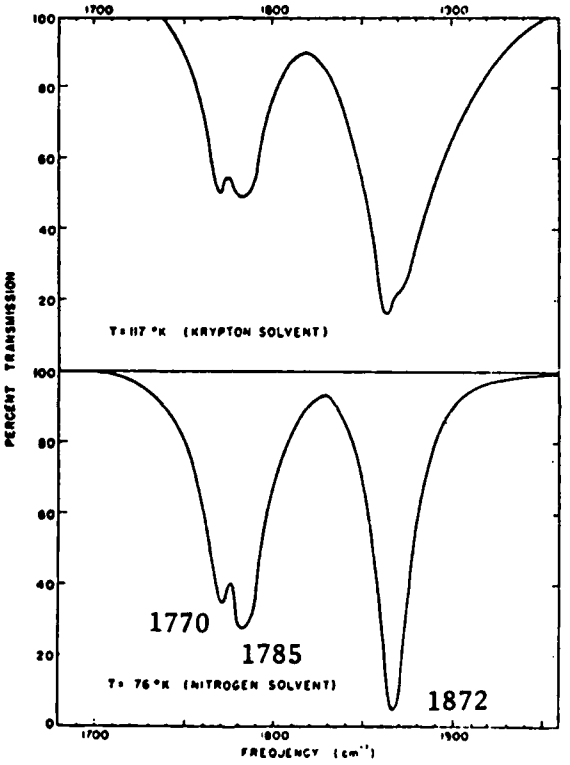

Spectra of nitric oxide solutions.

Figure 9. Infrared spectra of condensed NO in an O_2 matrix from Smith and Guillory (1977).

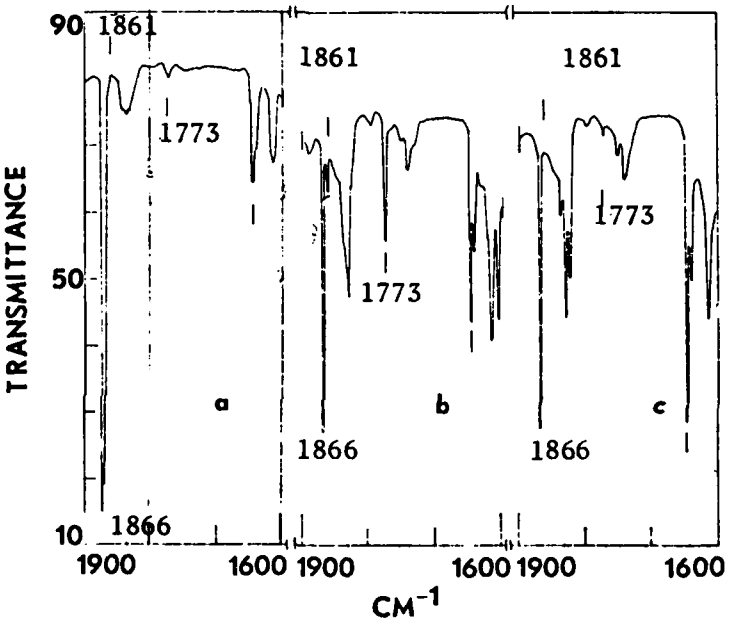

, O_2/NO ~180: (a) immediately after deposition; (b) immediately after warming to 32 K and recooling to 13 K; (c) after ~40 min at 13 K. The solid bars in each trace mark 1861, 1773, and 1644 cm^{-1}.

Figure 10. Infrared spectra of condensed O_2 as a function of temperature (CaF_2 transmission windows).

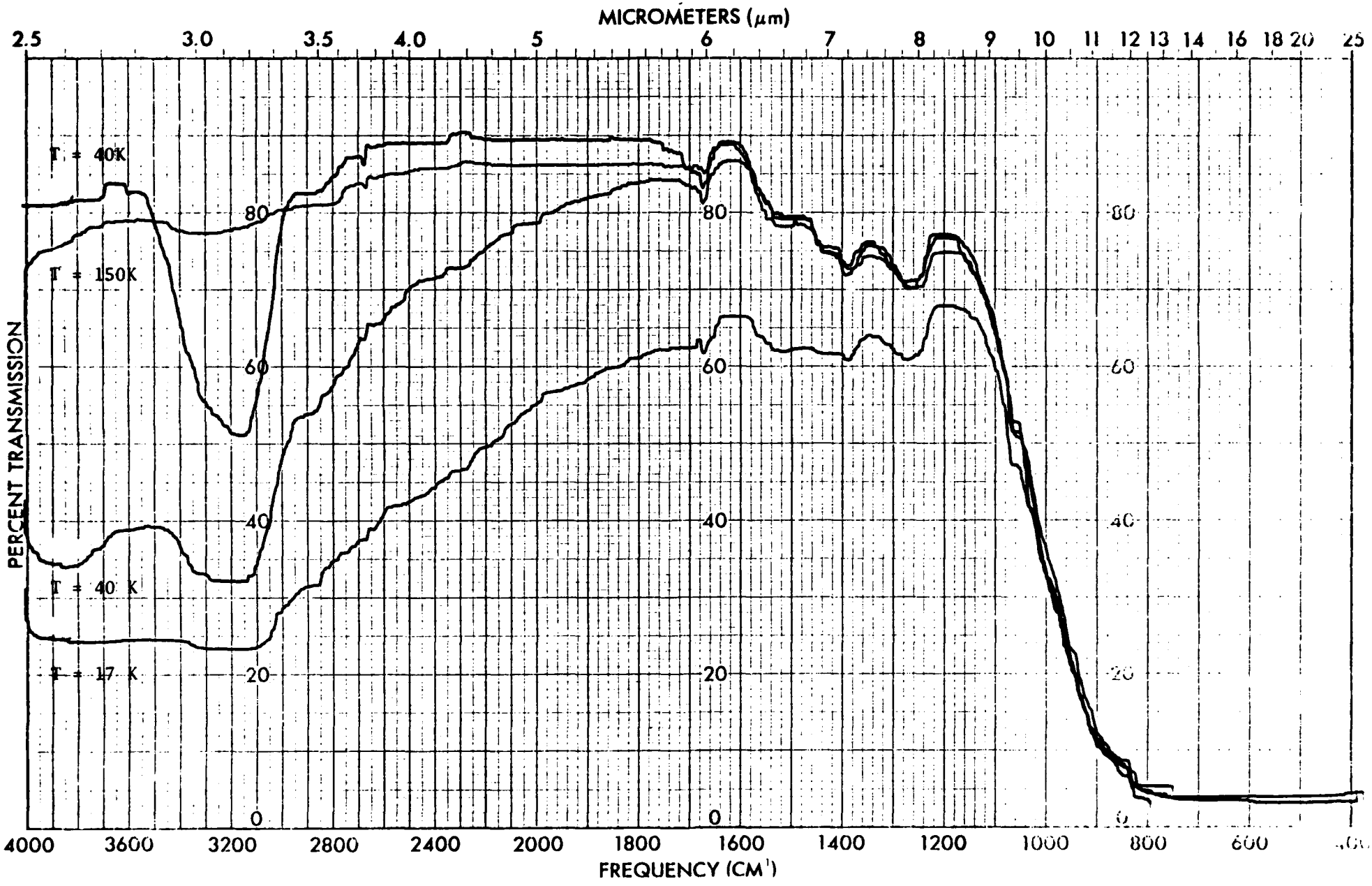
MICROMETERS (μm)
2.5
3.0
3.5
4.0
5
6
7
8
9
10
11
12
13
14
16
18
20
25
T = 40K
T = 150K
T = 40 K
T = 17 K
PERCENT TRANSMISSION
80
60
40
20
0
4000
3600
3200
2800
2400
2000
1800
1600
1400
1200
1000
800
600
FREQUENCY (CM⁻¹)

Figure 11. Infrared spectra of a 2.5 mol% O_3 in O_2 mixture as a function of temperature (CaF_2 transmission windows).

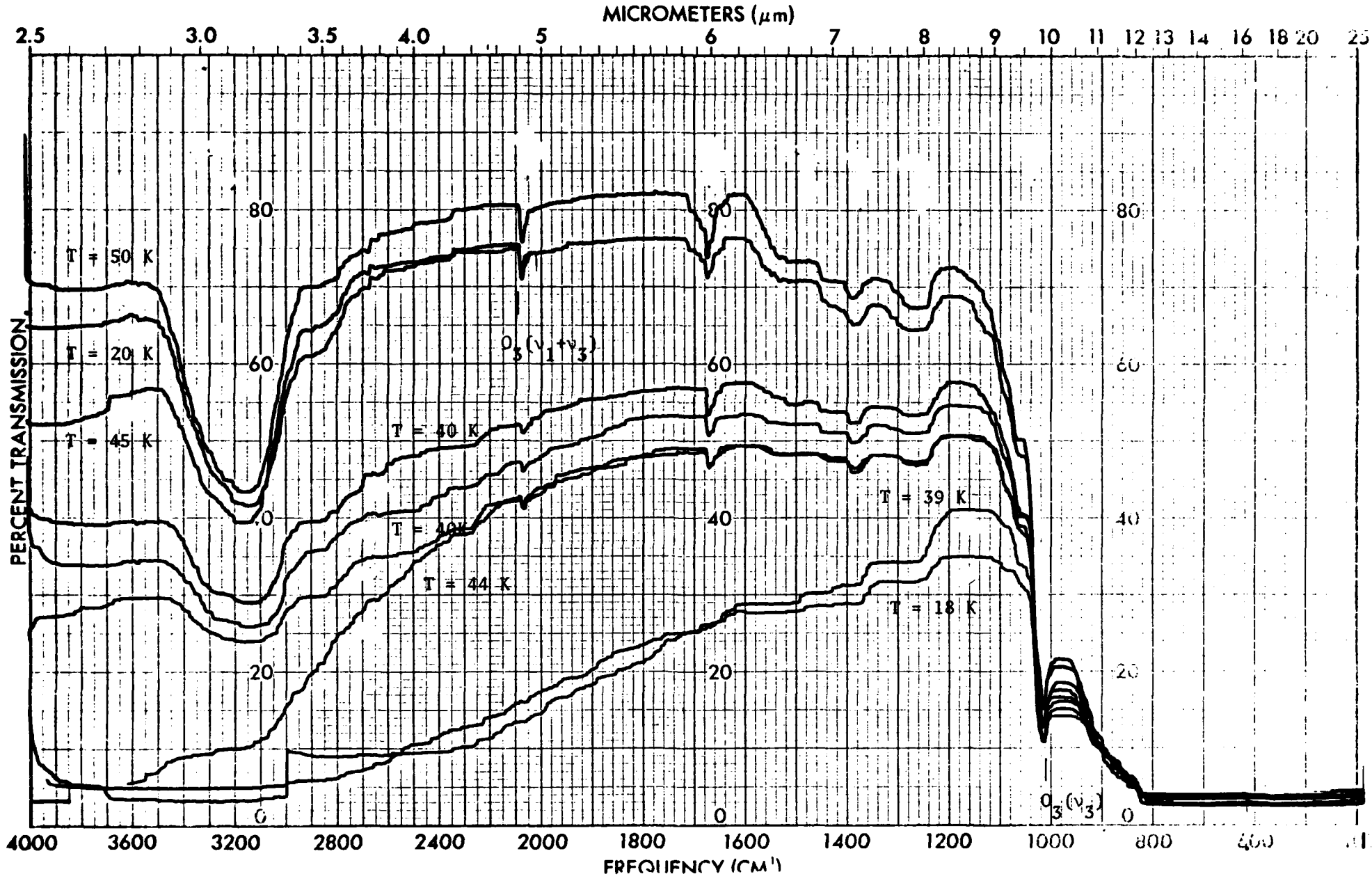
MICROMETERS (μm)
2.5
3.0
3.5
4.0
5
6
7
8
9
10
11
12
13
14
16
18
20
25
PERCENT TRANSMISSION
80
60
40
20
0
T = 50 K
T = 20 K
T = 45 K
T = 40 K
T = 40K
T = 44 K
T = 39 K
T = 18 K
$O_3(\nu_1+\nu_3)$
$O_3(\nu_3)$
4000
3600
3200
2800
2400
2000
1800
1600
1400
1200
1000
800
FREQUENCY (CM^{-1})

Figure 12. Concentration of condensed O_3 from a 2.5 mol% O_3 in O_2 mixture (CdTe transmission windows).

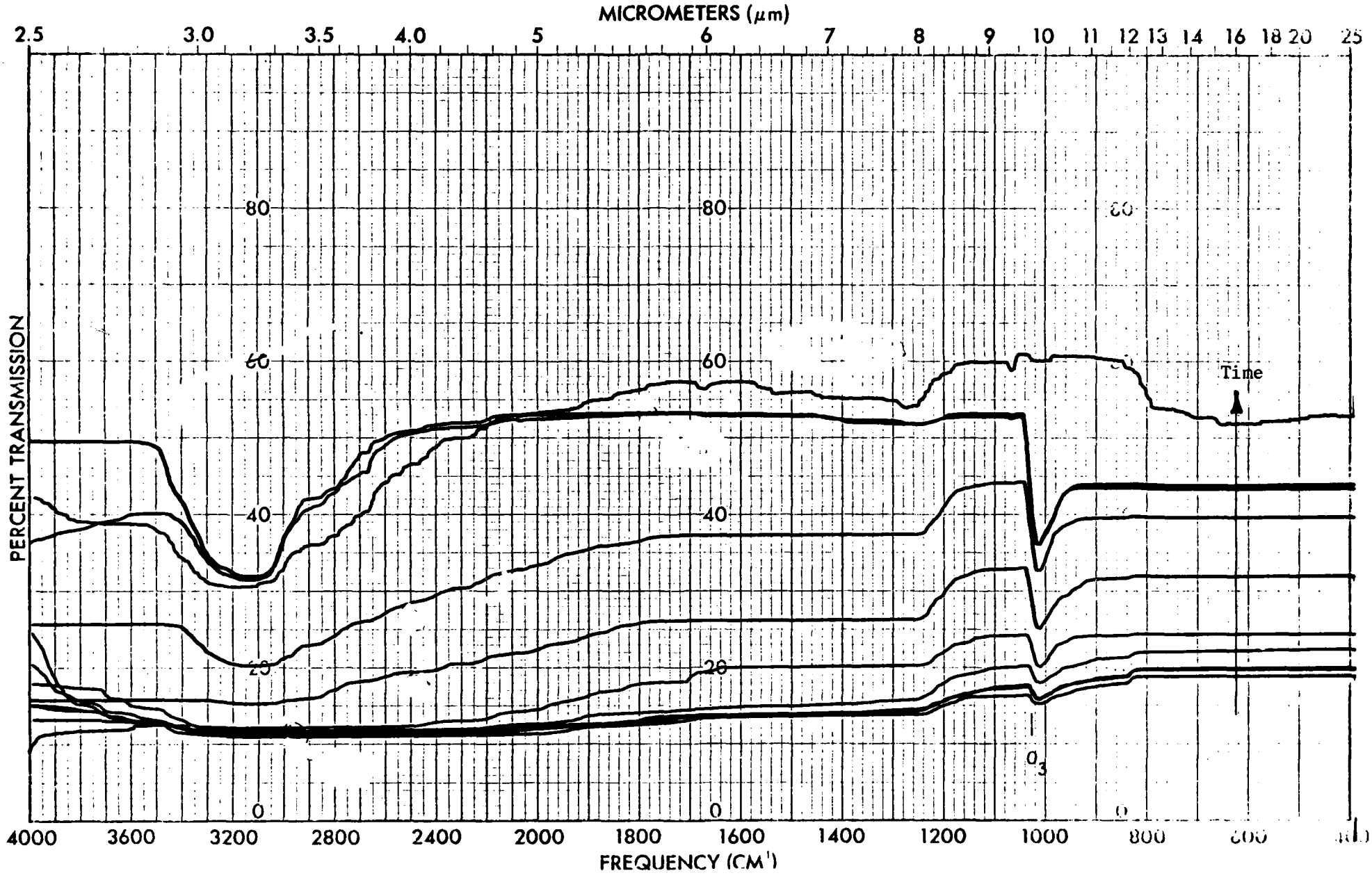
MICROMETERS (μm)
2.5
3.0
3.5
4.0
5
6
7
8
9
10
11
12
13
14
16
18
20
25
PERCENT TRANSMISSION
80
60
40
20
0
Time
O_3
4000
3600
3200
2800
2400
2000
1800
1600
1400
1200
1000
800
FREQUENCY (CM^{-1})

Figure 13. Infrared spectra of condensed NO for T = 35 K (a), and T = 50 K (b) (CdTe transmission windows).

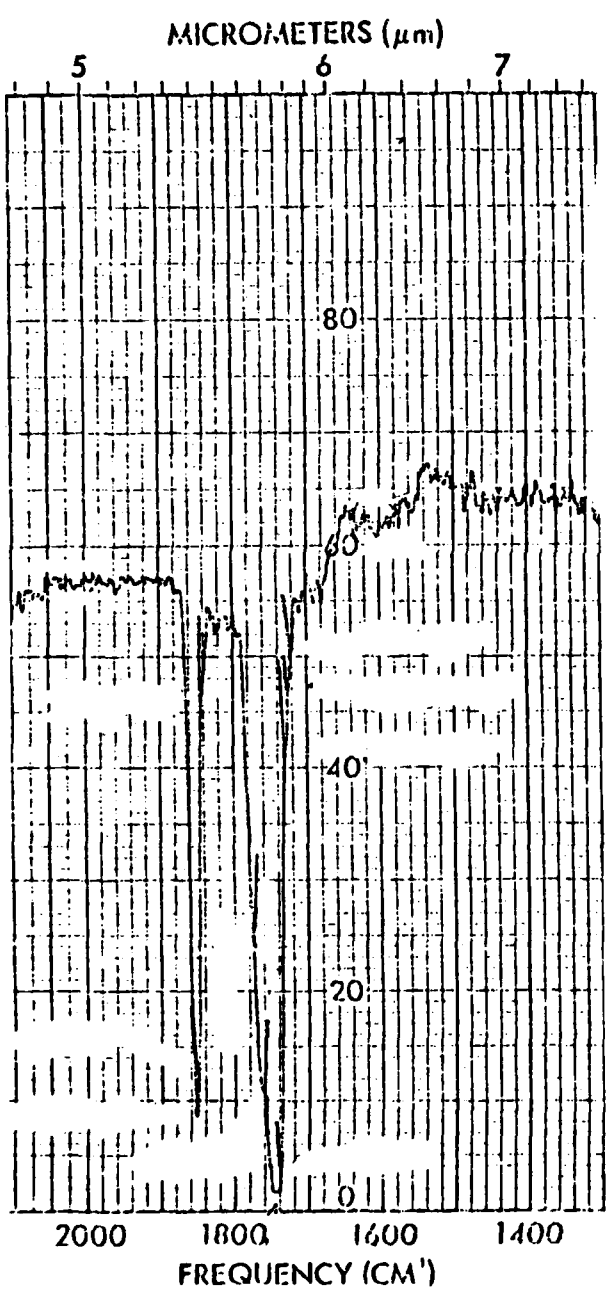
MICROMETERS (μm)
5
6
7
80
60
40
20
0
2000
1800
1600
1400
FREQUENCY (CM')

(a)

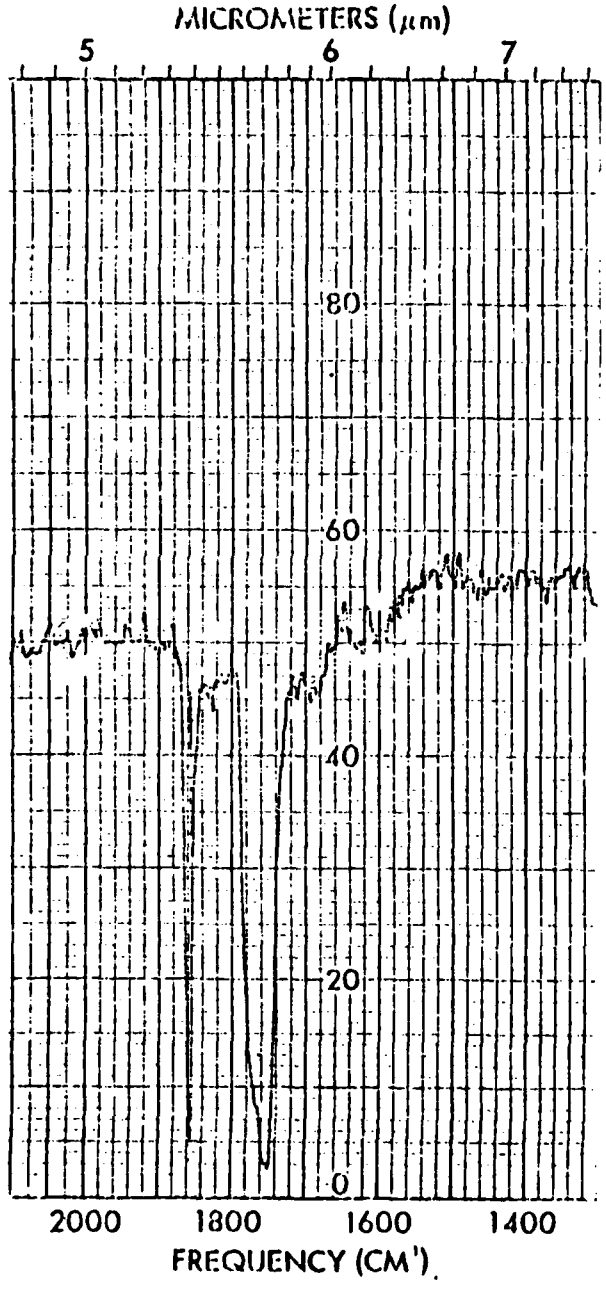
MICROMETERS (μm)
5
6
7
80
60
40
20
0
2000
1800
1600
1400
FREQUENCY (CM')

(b)

Figure 14. Behavior of the 1845 cm^{-1} absorption feature in condensed NO as a function of temperature.

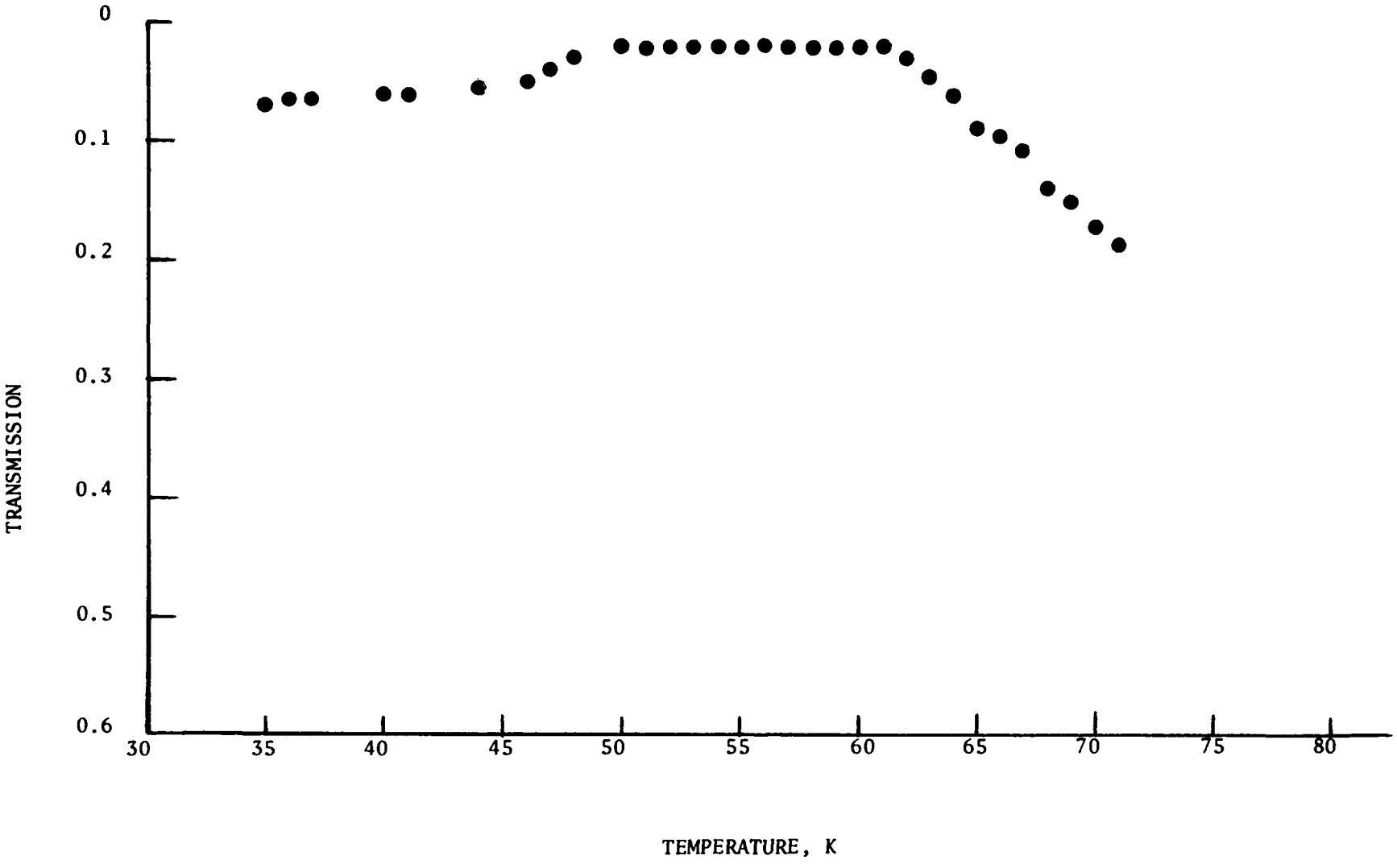
0
0.1
0.2
0.3
0.4
0.5
0.6
TRANSMISSION
30
35
40
45
50
55
60
65
70
75
80
TEMPERATURE, K

Figure 15. Mass spectrometric desorption spectra of NO for peaks m/e = 30 and 28 subsequent to deposition on gold-flashed stain less steel at 16 K. (from Calo et al., 1981).

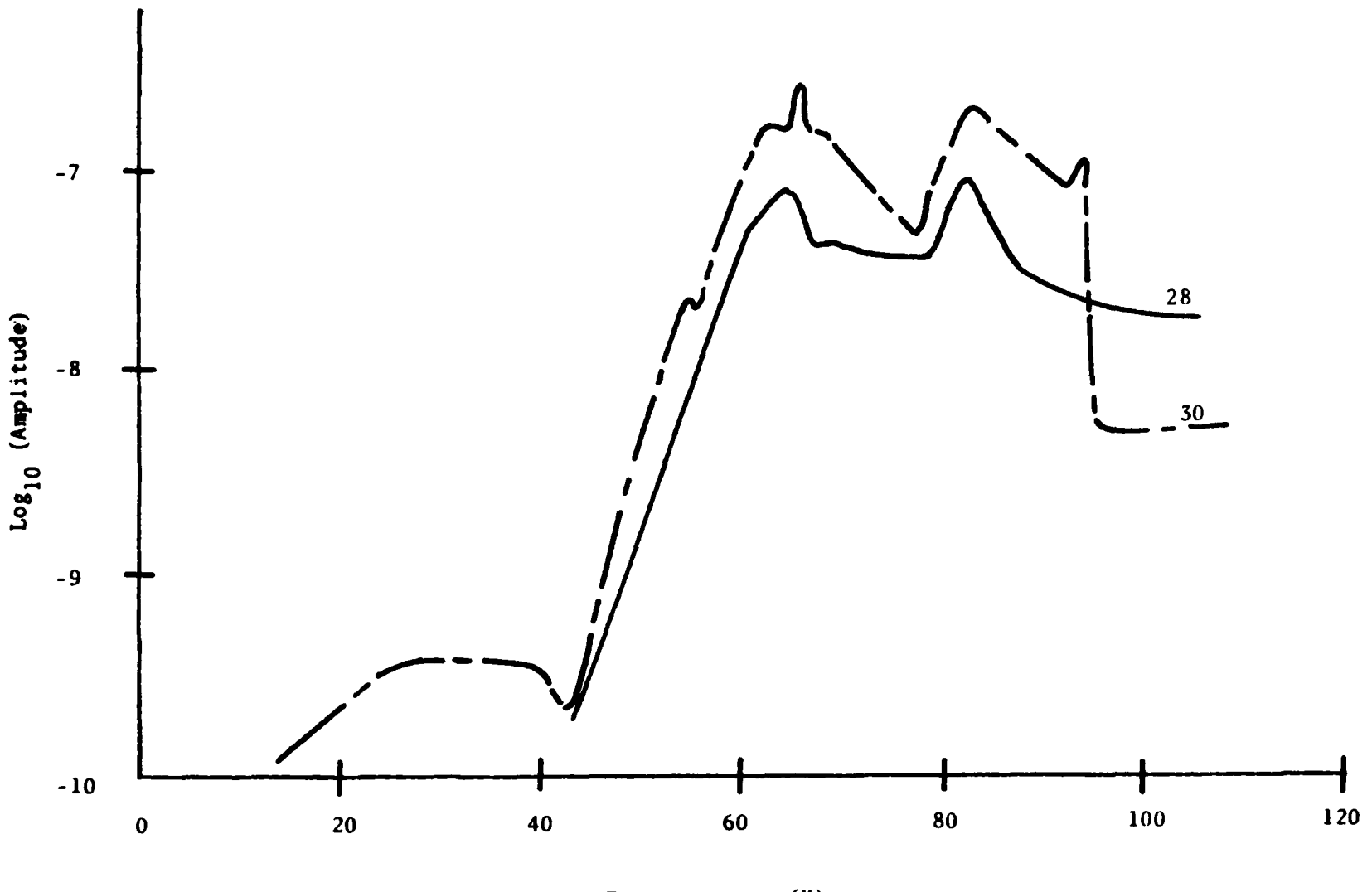
-7
-8
-9
-10
Log_{10} (Amplitude)
28
30
0
20
40
60
80
100
120
Temperature (K)

Figure 16. Infrared spectrum of condensed NO deposited on an O_3/O_2 substrate at 29 K (CaF_2 transmission windows).

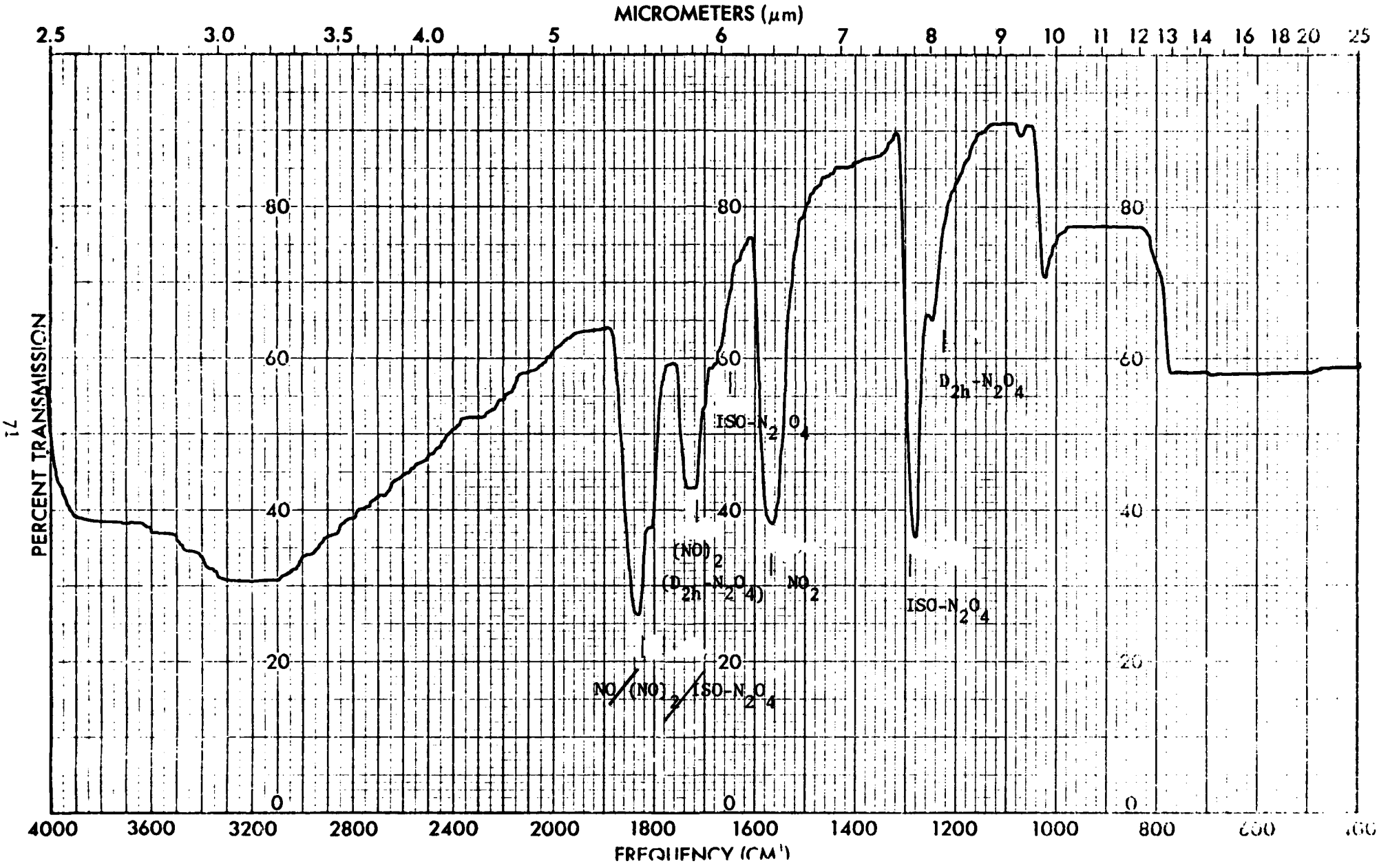
MICROMETERS (μm)
2.5
3.0
3.5
4.0
5
6
7
8
9
10
11
12
13
14
16
18
20
25
PERCENT TRANSMISSION
0
20
40
60
80
4000
3600
3200
2800
2400
2000
1800
1600
1400
1200
1000
800
FREQUENCY (CM⁻¹)
D2h-N2O4
ISO-N2O4
(NO)2
(D2h-N2O4)
NO2
ISO-N2O4
NO/(NO)2/ISO-N2O4

Figure 17. Infrared spectrum of the residual from the NO-O_3/O_2 sample in Figure 16 at 70 K (CaF_2 transmission windows).

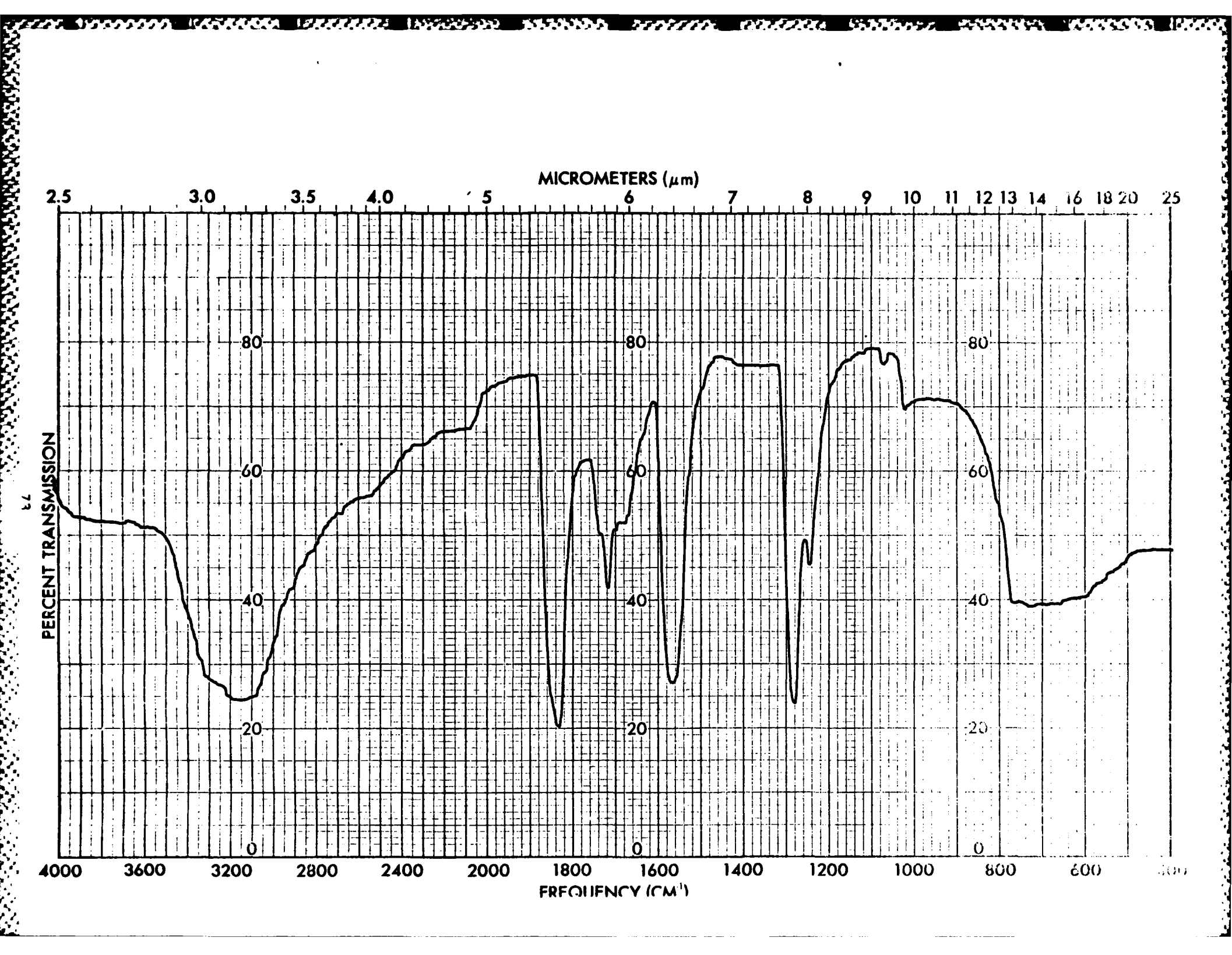
MICROMETERS (μm)
2.5
3.0
3.5
4.0
5
6
7
8
9
10
11
12
13
14
16
18
20
25
PERCENT TRANSMISSION
80
60
40
20
0
4000
3600
3200
2800
2400
2000
1800
1600
1400
1200
1000
800
600
FREQUENCY (CM⁻¹)

Figure 18. Photograph of apparatus for cryogenic immersion studies.

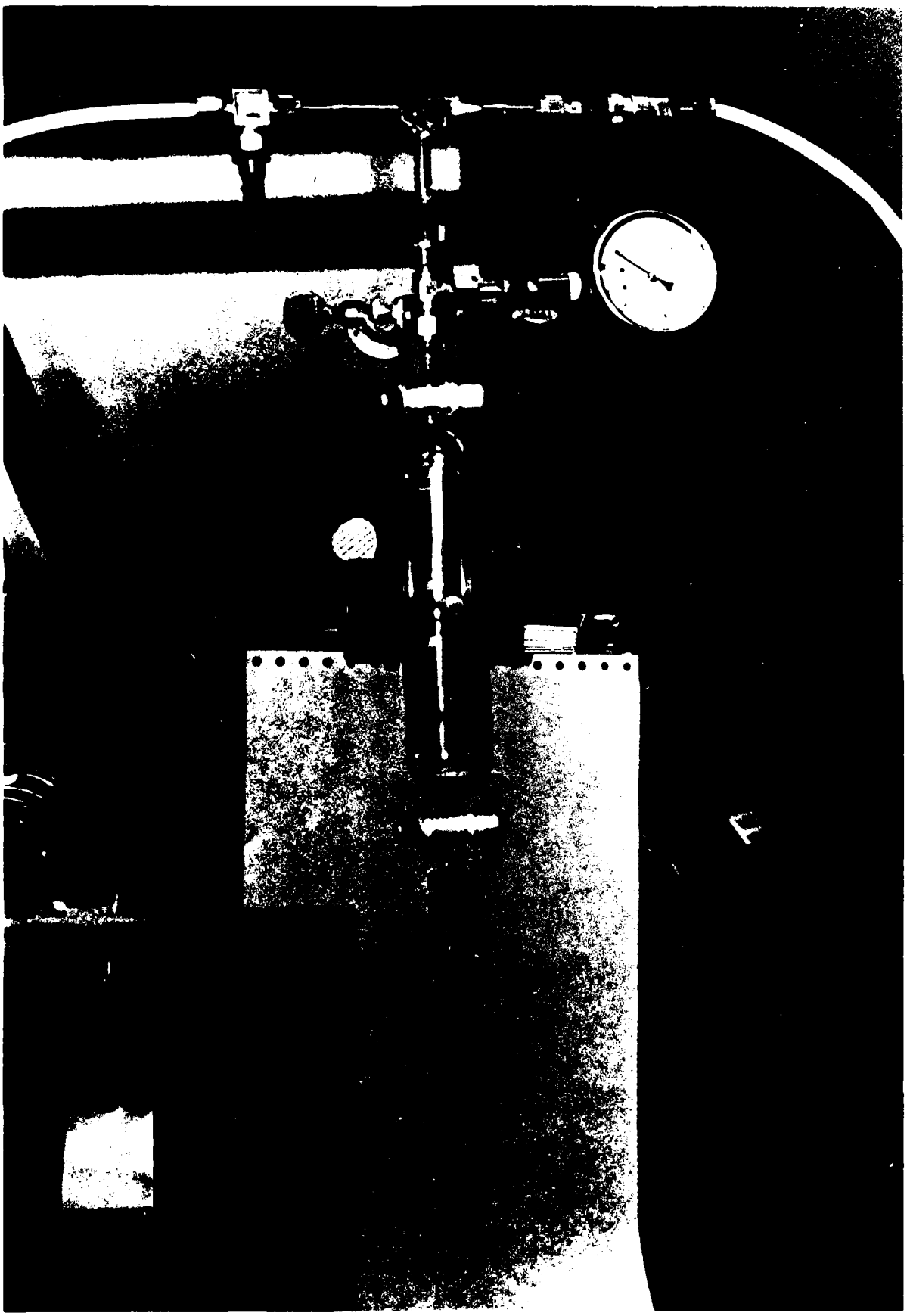

Figure 19. Photographs of cryogenic immersion studies with pure NO.

(c)

(b)

(a)

Figure 20. Photographs of cryogenic immersion studies with NO/O_2 mixtures.

(f)
(e)
(d)
(c)
(b)
(a)

Figure 21. NO conversion as a function of relative water content.

LEGEND:

- ● TYPE I.
- △ TYPE II.
- ▲ TYPE III.
- ○ TYPE IV.
- ■ TYPE V.
- □ TYPE VI.
- ◆ TYPE VII.

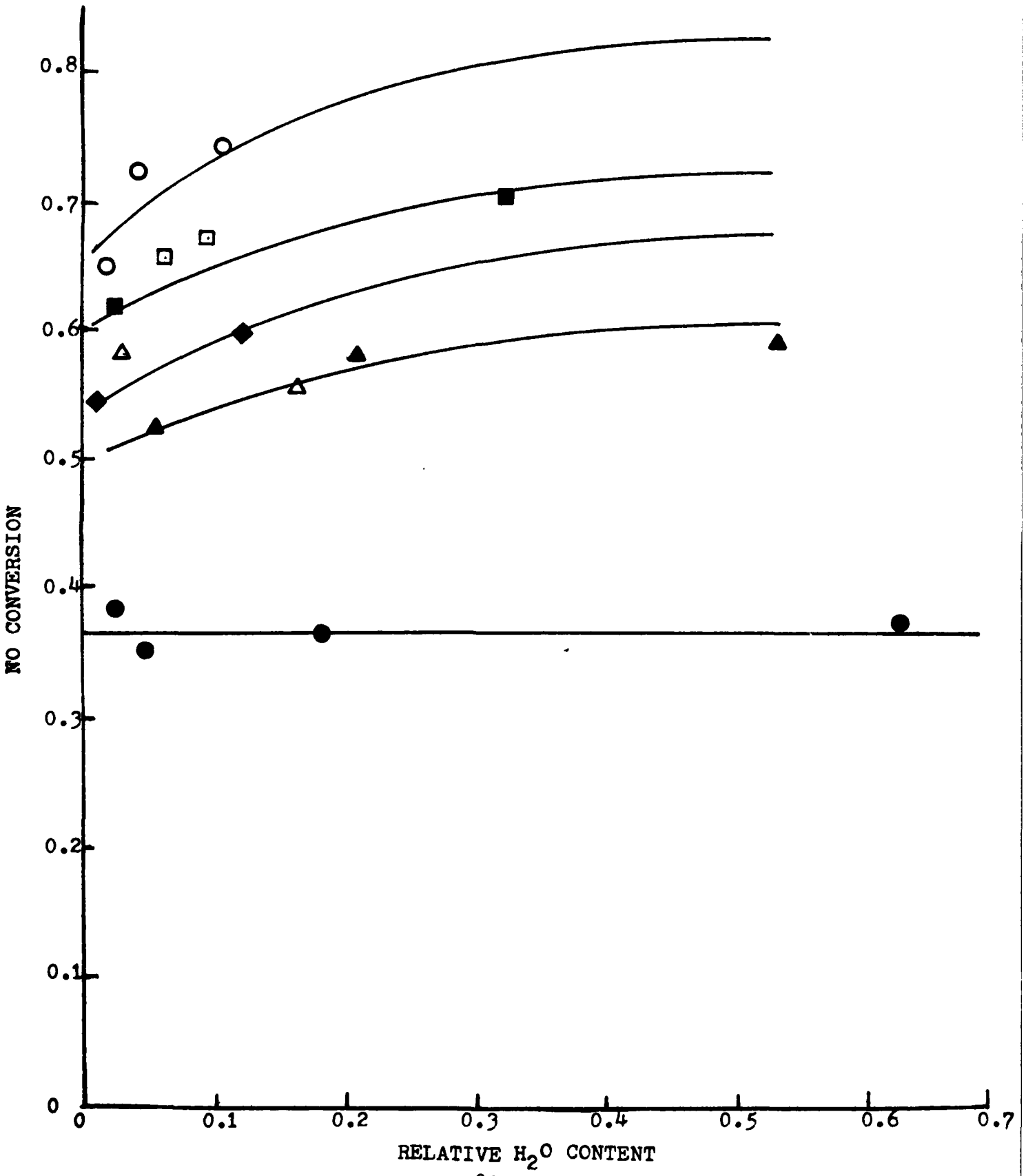
0.8
0.7
0.6
0.5
0.4
0.3
0.2
0.1
0
NO CONVERSION
0
0.1
0.2
0.3
0.4
0.5
0.6
0.7
RELATIVE H_2O CONTENT

Figure 22. Infrared spectrum of condensed NO/O_2 sample at 24K; Run 22, Type IV (see Table III).

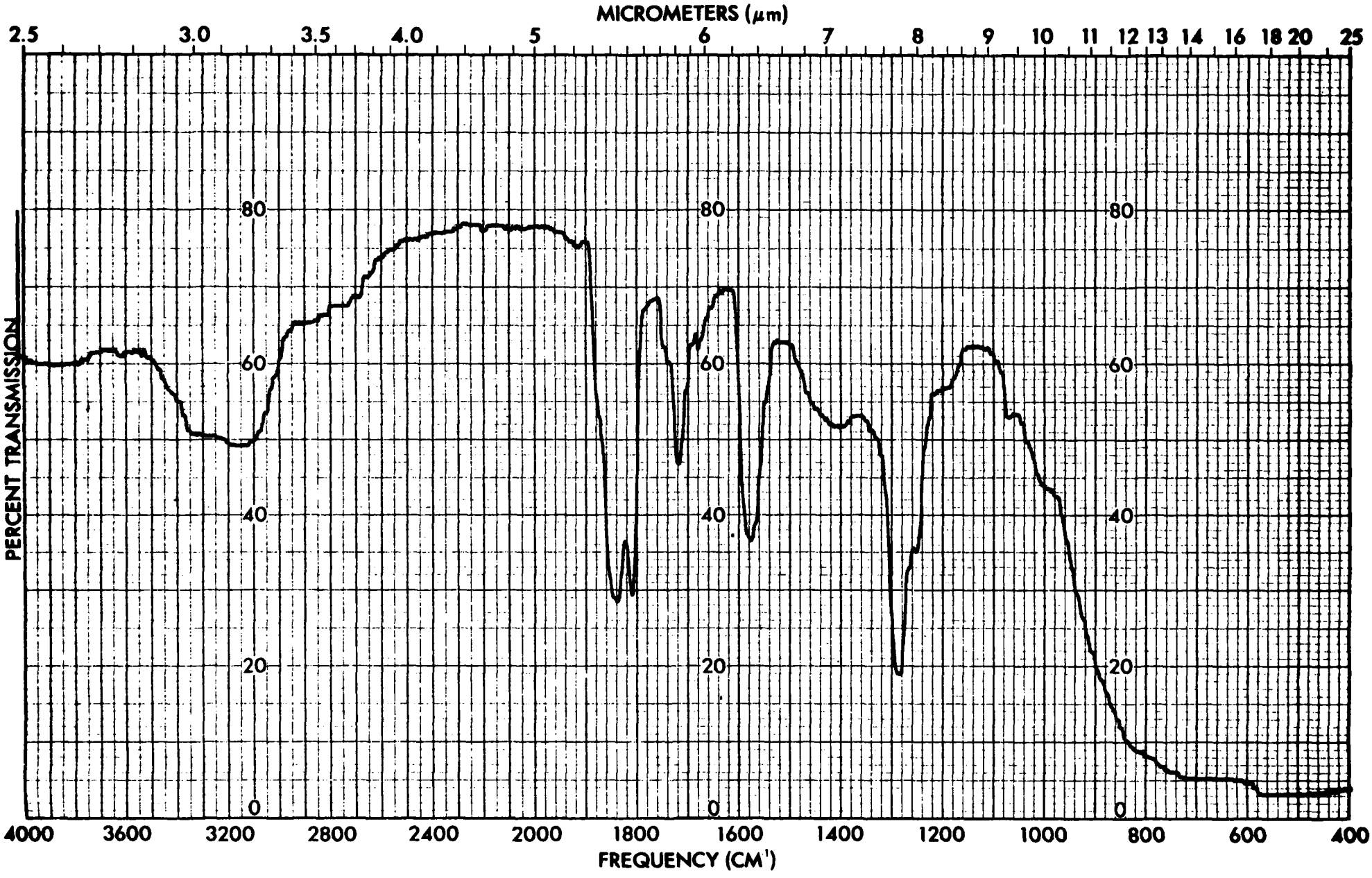
MICROMETERS (μm)
2.5
3.0
3.5
4.0
5
6
7
8
9
10
11
12
13
14
16
18
20
25
PERCENT TRANSMISSION
80
60
40
20
0
4000
3600
3200
2800
2400
2000
1800
1600
1400
1200
1000
800
600
400
FREQUENCY (CM⁻¹)

Appendix A.

EXPERIMENTAL APPARATUS

A.1. Sample Cell.

The heart of the experimental apparatus was the IR transmission window/cryosurface. In the current work, this window was a polycrystalline CdTe disk, 1 in. in diameter and 0.125 in. in thickness (~65% transmission, 4000-400 cm^{-1}). This window was clamped in a copper holder assembly (see Figure A-1), which was in turn screwed into the cold end of a closed-cycle, helium refrigerator (Air Products Displex CS202). Good thermal contact was insured by the insertion of indium strips between the contact surfaces. The window temperature was monitored by a silicon diode sensor and digital thermometer/controller (Lake-Shore Cryotronics, DRC-7C).

The refrigerator expander and window holder assembly were enclosed in a vacuum shroud (see Figure A-2). This shroud was constructed from a standard 2.5 in. Excelon clear PVC tee machined to the dimensions indicated in Figure A-2. Two standard 2.5 in. PVC end caps were machined to accomodate the two IR transmission windows (for the entering and exiting IR beam) which were cemented to the ends of the straight run of the tee. Two different types of transmission windows were used on the cell during the current work: CaF$_2$ (typical background spectrum in Figure A-3; ~900 cm^{-1} cutoff), and CdTe (typical background spectrum given in Figure A-4). Both types were 1 in. diameter disks, 0.125 in. thick.

The vacuum shroud is evacuated by a mechanical pump (Alcatel

2030, 425 l/min) baffled with a molecular sieve trap. In order to control the water vapor background in the vicinity of the sample window, it was found necessary to be able to cryogenically pump the vacuum shroud. This was accomplished with another closed-cycle, helium refrigerator (Air Products Displex CS208L). This refrigerator and the two sample gas inlets were interfaced to the vacuum shroud via a specially-constructed manifold, shown in the photographs in Figure A-5. This manifold allows for the separate, simultaneous deposition of two gas samples and for the evacuation of the vacuum shroud by the auxiliary cryogenic refrigerator. The entire apparatus is shown in the assembly photograph in Figure A-6. The auxiliary refrigerator could also be used as a source of cold, dry helium gas to enable purging of the sample window before and during sample deposition to minimize accumulation of water vapor and other contaminants. The cold helium purge gas was produced from a gas cylinder of helium that was was passed through a copper heat exchanger, packed with copper shot that was mounted on the cold end of the auxiliary refrigerator.

The entire cryogenic refrigerator/vacuum schroud assembly was aligned and positioned in the beam of a PerKin-Elmer 735B infrared spectrophotometer. The spectrophotometer was calibrated against a standard polystyrene sample (see Figure A-7), and in the single beam, calibrate mode on a background water vapor spectrum (see Figure A-8).

Sample gases were admitted to the system via the manifold shown in the photographs in Figure A-5. Both sample tubing inlets terminated at the circumference of the circular opening in the

copper window holder such that the sample gases flowed past close and parallel to the window surface. This mode of deposition resulted in a good, even coating of condensate over most of the window area.

A.2. NO_x Chemiluminescence Analyzer.

A ThermoElectron Model 10AR NO_x chemiluminescence analyzer was used to determine NO/NO_x ratios of desorbed samples and sample gases. The operating principle of the analyzer relies on the reaction between ozone and NO to produce electronically excited nitrogen dioxide. Emission from this species is monitored with a photomultiplier tube and related to the absolute concentration of NO via a calibration procedure. In order to determine the concentration of total NO_x in the sample, the gas sample is first passed through a stainless steel reactor maintained at 650 °C which quantitatively reduces NO_x to NO for detection using the ozone reaction exactly as in the NO mode.

A.3. Welsbach Ozonator.

Ozone was produced as an ozone-oxygen mixture in a model T-408 Welsbach high voltage discharge ozonator. To insure reproducibility of ozone concentrations, the ozonator was always set at an oxygen feed rate of 2 SLPM (standard liters per minute) at 8 psig, and only the primary voltage was varied to change the ozone concentration.

The ozonator was calibrated using a standard analytical technique. A schematic of the calibration apparatus is presented in Figure A-9. The materials employed were limited to glass, stainless steel, teflon, and tygon, as recommended by the

manufacturer. As shown in Figure A-9, the bulk of the ozonated oxygen was fed to a scrubber charged with a potassium iodide solution which chemically destroys ozone. A slipstream from the ozonator output was fed to a gas bubbler (medium porosity) containing 400 ml of 2% potassium iodide solution at approximately 0.3 l/min. In the bubbler, the reaction:

$$O_3 + 2I^- + H_2O \longrightarrow O_2 + I_2 + 2OH^-$$

takes place. The gas, now stripped of ozone, passes through a pressure gauge and then through a wet test meter, where its volume was recorded as a function of time. The iodine solution produced in the bubbler is then removed and acidified with 10 ml of 1M sulfuric acid, and titrated with either 0.1N or 0.01N sodium thiosulfate solution, depending on the expected concentration of the iodine solution. Starch solution was used as the indicator and is added when the bright yellow color of the solution begins to fade.

The data obtained from this procedure allowed the determination of ozone concentrations in the sample gas stream. The manufacturer of the ozonator claims that this calibration procedure is accurate ±1% of the amount of ozone in the sample stream down to concentrations of approximately 28 ppm.

Using this calibration procedure, the ozone contration in the oxygen stream was calibrated against the primary voltage of the Welsbach ozonator. It was found that high ozone concentrations up to 2.5% could be delivered reproducibly. This latter concentration was used in the current work.

Figure A-1. IR window holder assembly.

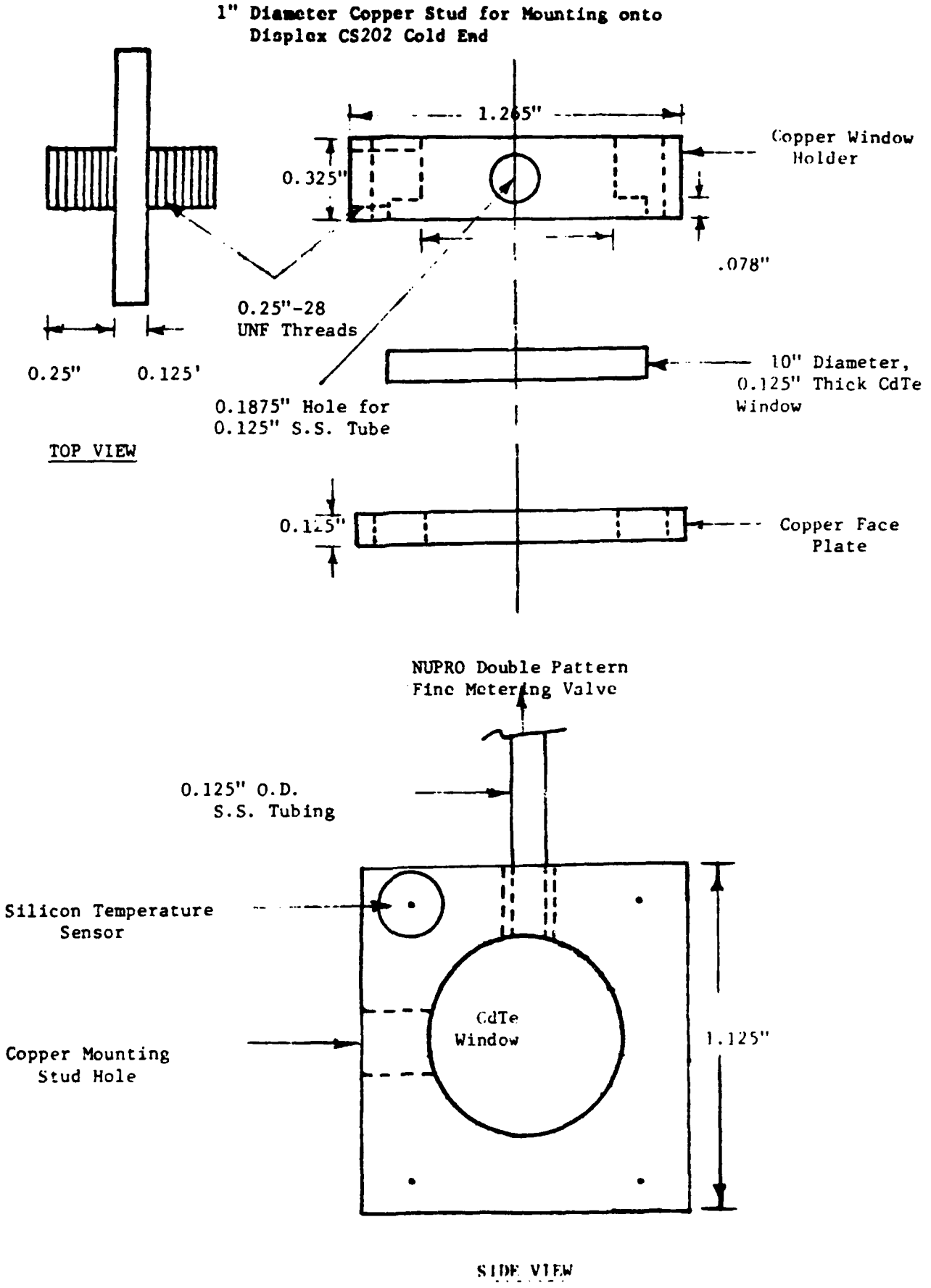
1" Diameter Copper Stud for Mounting onto
Displex CS202 Cold End
1.265"
Copper Window
Holder
0.325"
.078"
0.25"-28
UNF Threads
0.25"
0.125'
10" Diameter,
0.125" Thick CdTe
Window
0.1875" Hole for
0.125" S.S. Tube
TOP VIEW
0.125"
Copper Face
Plate
NUPRO Double Pattern
Fine Metering Valve
0.125" O.D.
S.S. Tubing
Silicon Temperature
Sensor
CdTe
Window
Copper Mounting
Stud Hole
1.125"
SIDE VIEW

AD-A137 879 CHEMICAL REACTIONS AND MOLECULAR AGGREGATION IN CRYOGENIC WHOLE AIR SAMPL..(U) BROWN UNIV PROVIDENCE RI DIV OF ENGINEERING J M CALO ET AL. JUL 83 2/2

UNCLASSIFIED AFGL-TR-83-0235 F19628-81-C-0157 F/G 4/1 NL

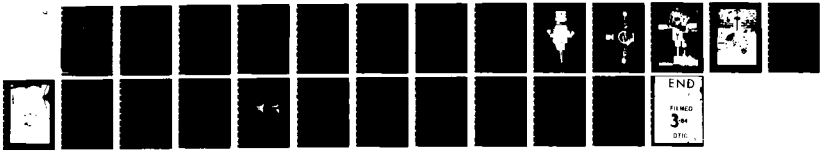

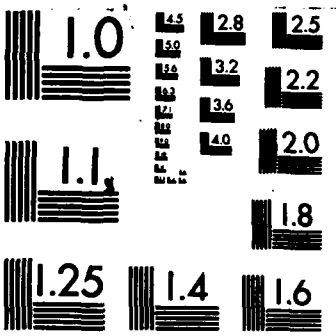

MICROCOPY RESOLUTION TEST CHART
NATIONAL BUREAU OF STANDARDS-1963-A

Figure A-2. PVC vacuum shroud schematic.

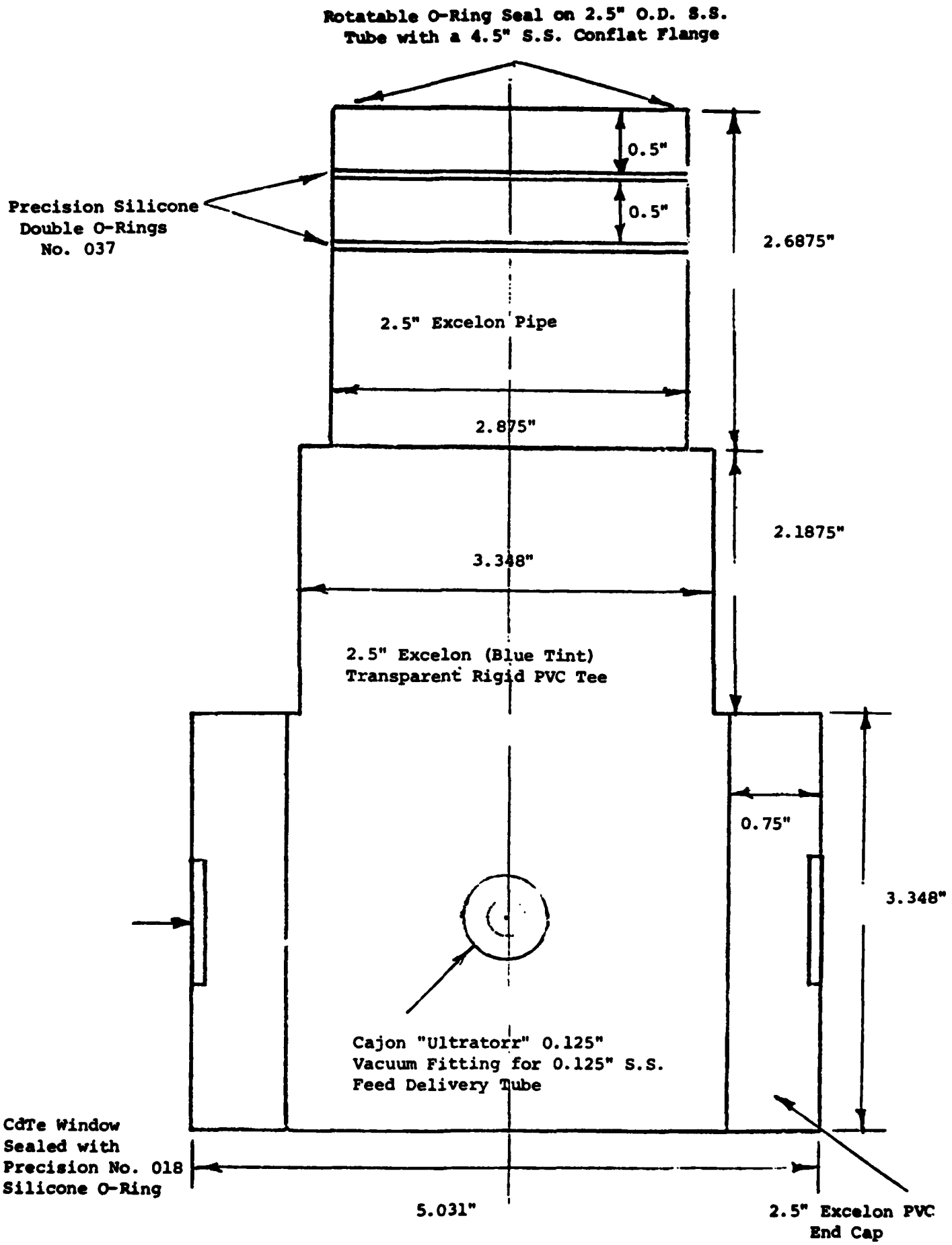
Rotatable O-Ring Seal on 2.5" O.D. S.S.
Tube with a 4.5" S.S. Conflat Flange
0.5"
0.5"
Precision Silicone
Double O-Rings
No. 037
2.6875"
2.5" Excelon Pipe
2.875"
2.1875"
3.348"
2.5" Excelon (Blue Tint)
Transparent Rigid PVC Tee
0.75"
3.348"
Cajon "Ultratorr" 0.125"
Vacuum Fitting for 0.125" S.S.
Feed Delivery Tube
CdTe Window
Sealed with
Precision No. 018
Silicone O-Ring
5.031"
2.5" Excelon PVC
End Cap

Figure A-3. Typical background infrared spectrum with CaF_2 transmission windows.

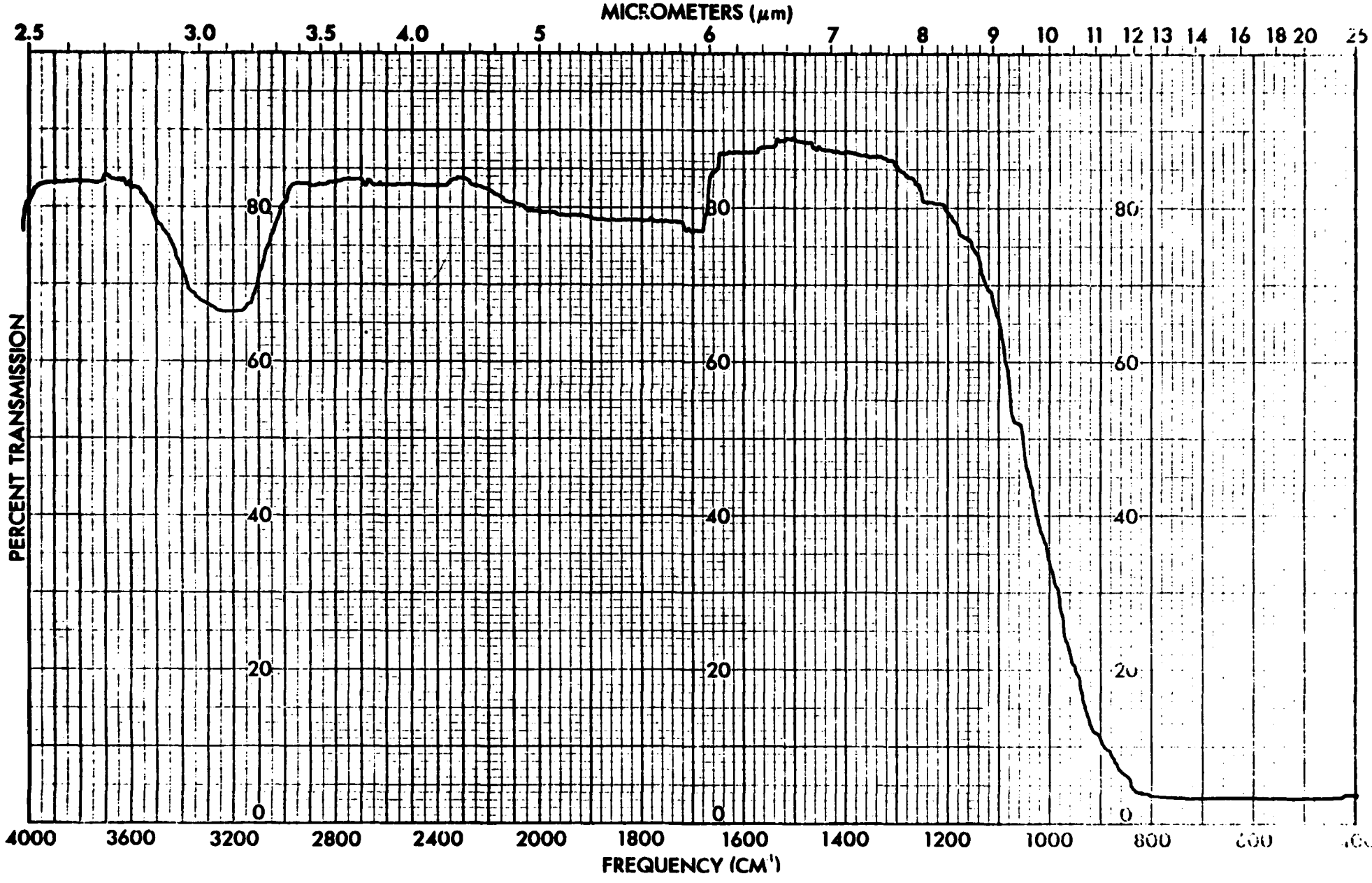
MICROMETERS (μm)
2.5
3.0
3.5
4.0
5
6
7
8
9
10
11
12
13
14
16
18
20
25
PERCENT TRANSMISSION
80
60
40
20
0
4000
3600
3200
2800
2400
2000
1800
1600
1400
1200
1000
800
FREQUENCY (CM⁻¹)

Figure A-4. Typical background infrared spectrum with CdTe transmission windows.

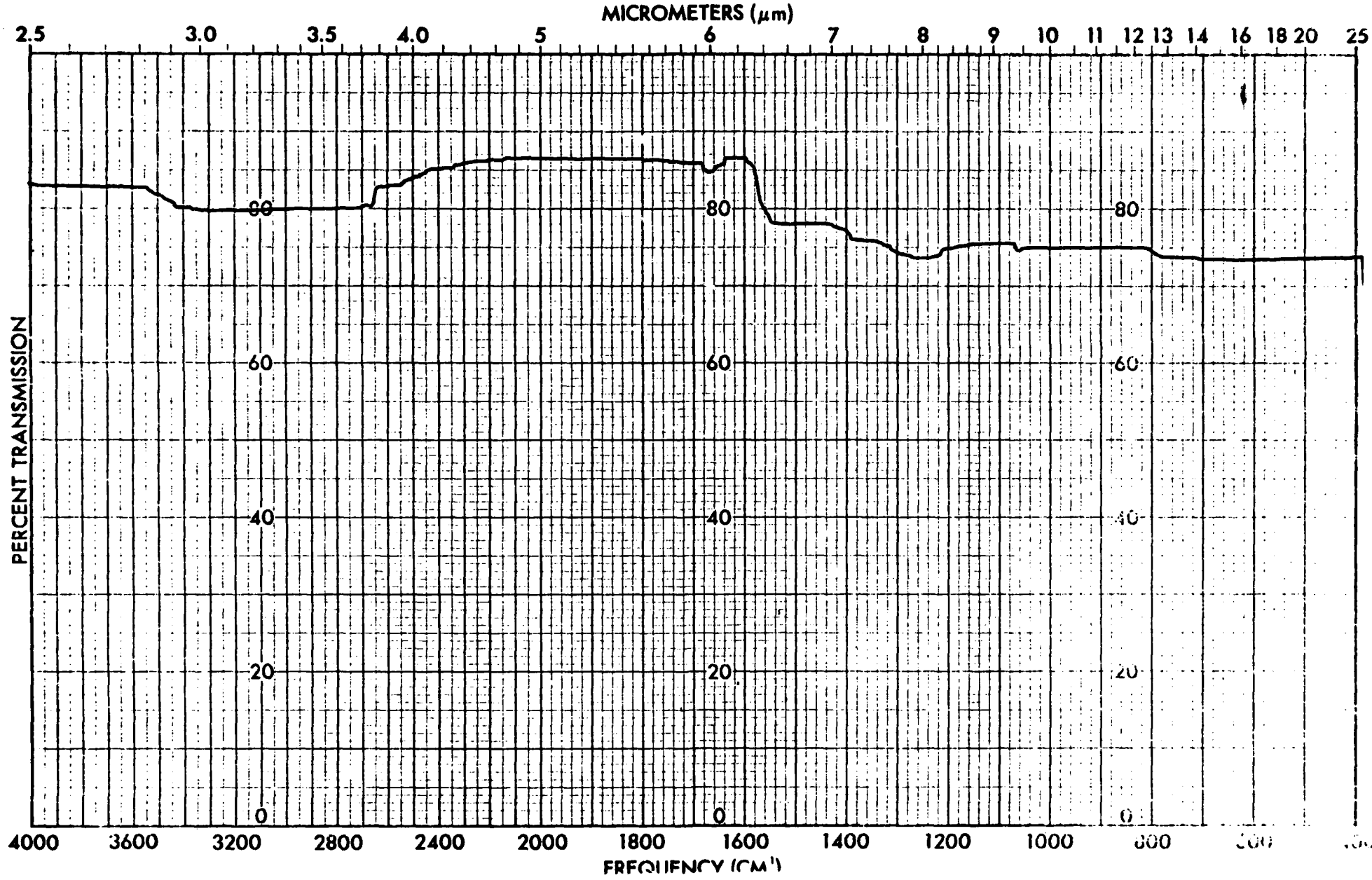
MICROMETERS (μm)
2.5
3.0
3.5
4.0
5
6
7
8
9
10
11
12
13
14
16
18
20
25
PERCENT TRANSMISSION
100
80
60
40
20
0
4000
3600
3200
2800
2400
2000
1800
1600
1400
1200
1000
800
FREQUENCY (CM⁻¹)

Figure A-5. Photographs of the inlet manifold:

(a) Side view, disconnected from apparatus showing deposition flow tubes and fittings.

(b) Top view through auxiliary cryopump connection, disconnected from apparatus.

(c) Side view, connected to the apparatus ; i.e., to the auxiliary cryopump, flow metering valves, and copper block sample window holder.

(d) Front view, connected to the apparatus.

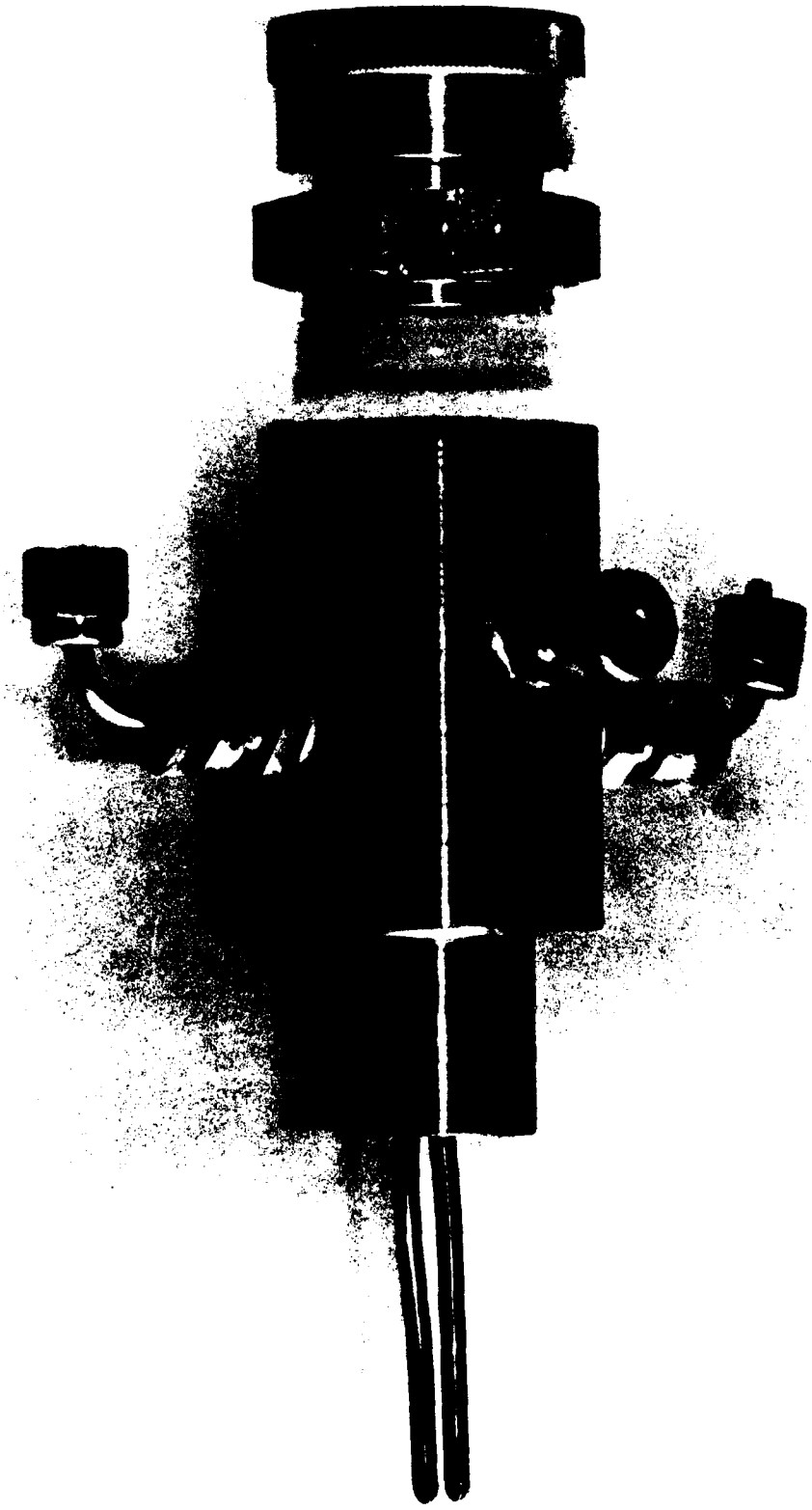

(a)

(a)

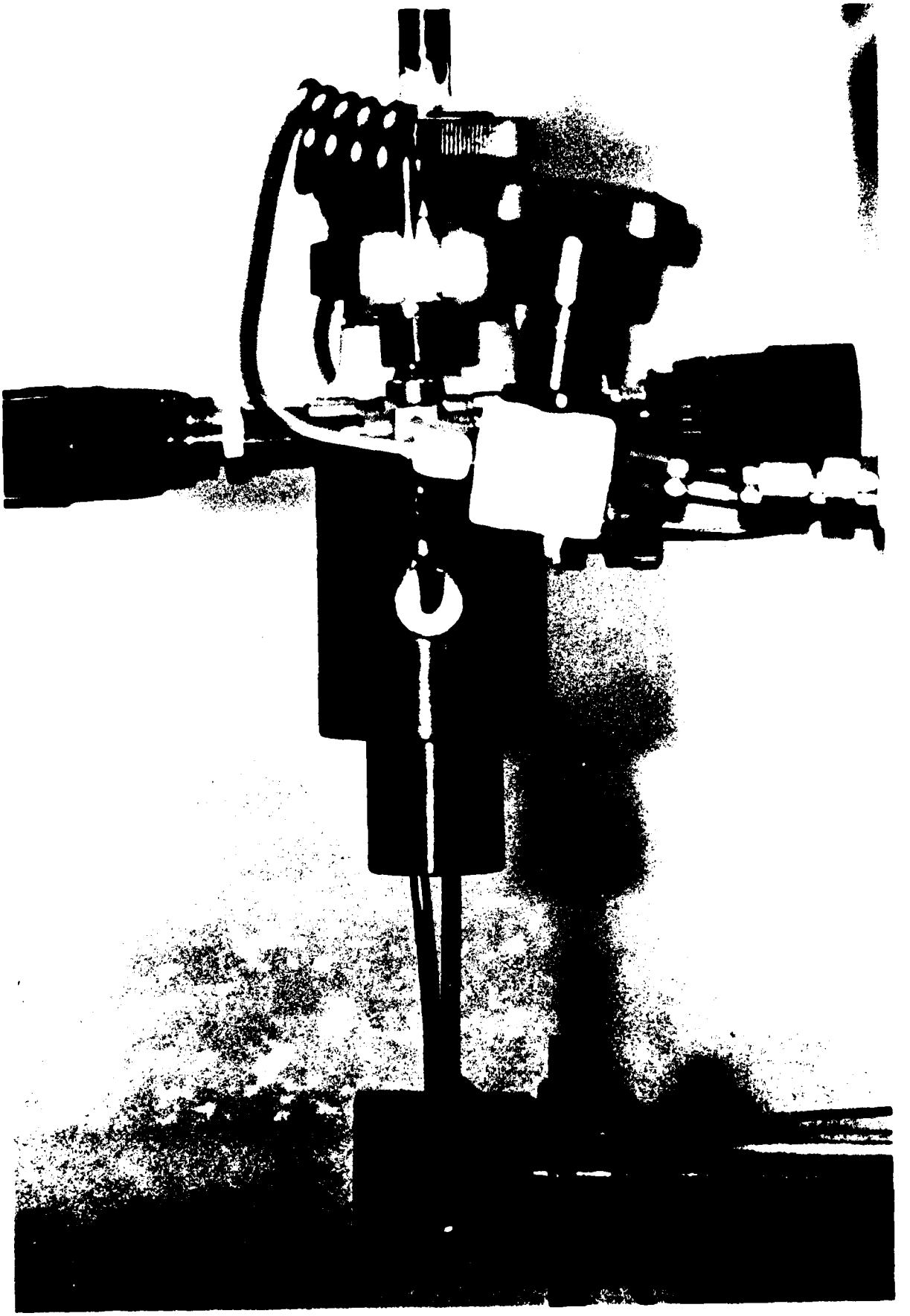

(c)

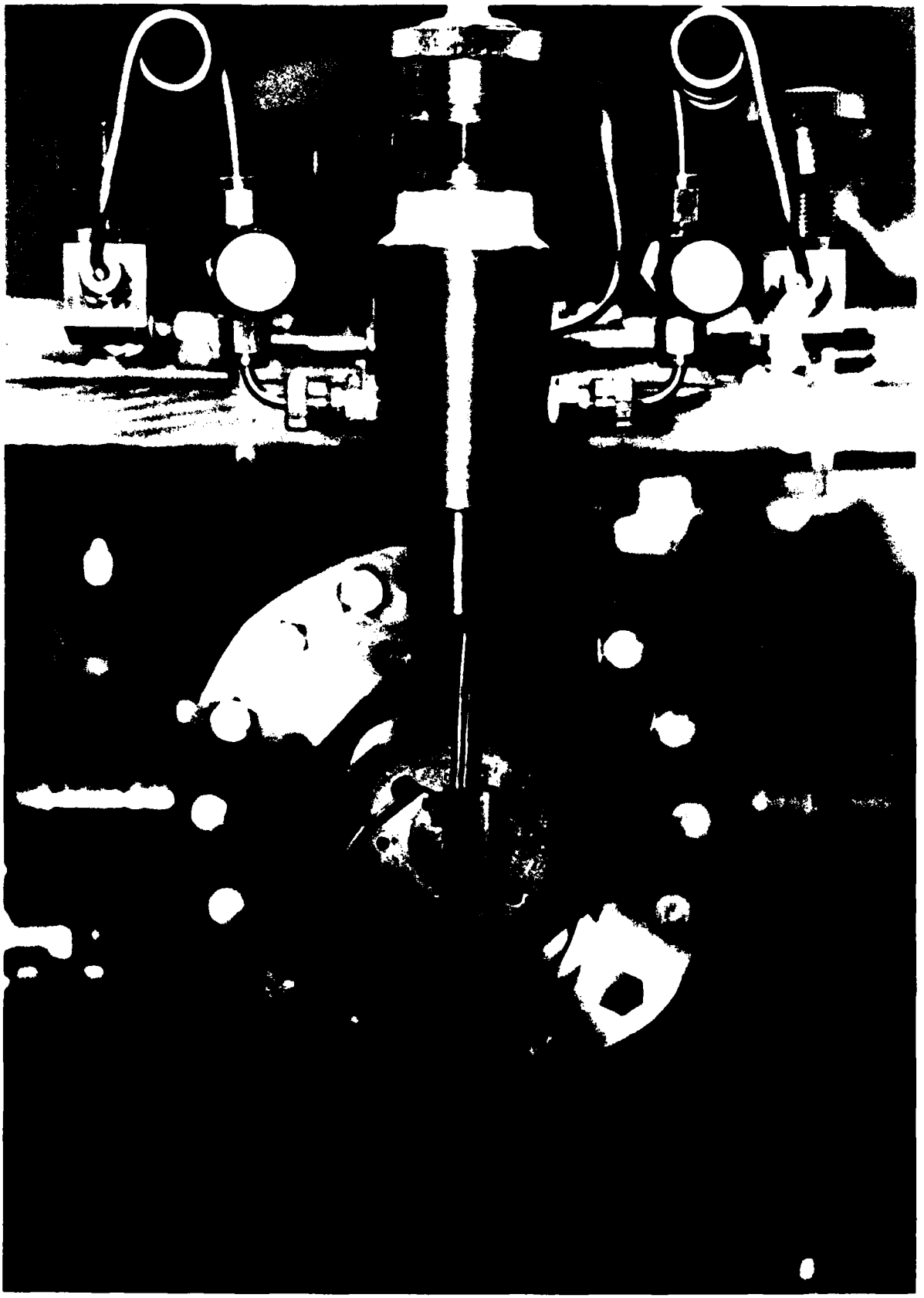

(d)

Figure A-6. Photograph of the assembled apparatus.

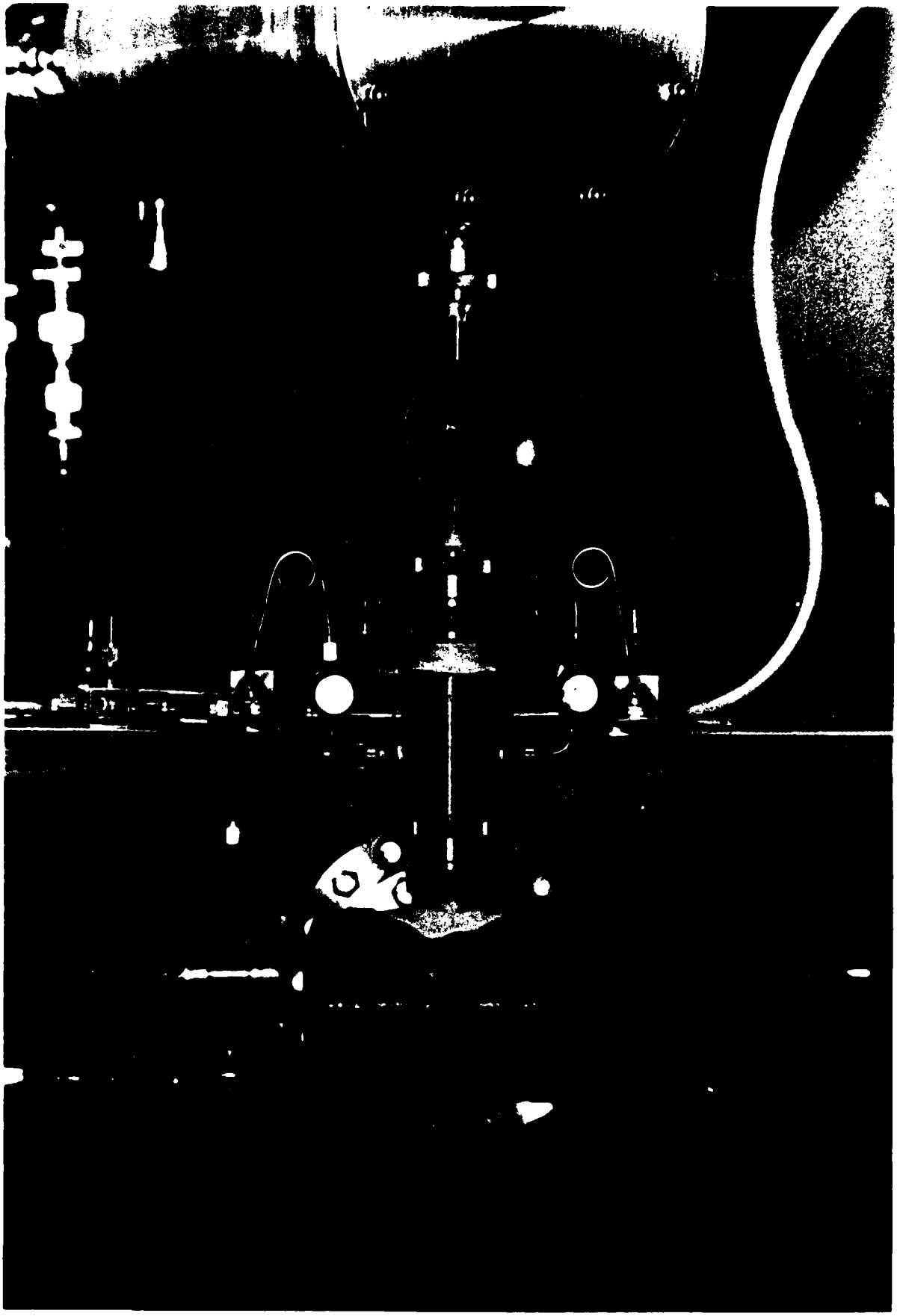

Figure A-7. Infrared spectrum of standard polystyrene calibration film inserted between vacuum shroud window and infrared detector (Cell: T=300K, P< 1 mtorr). Inset: polystyrene test spectrum from Perkin-Elmer 735B instrument manual. (CdTe transmission windows.)

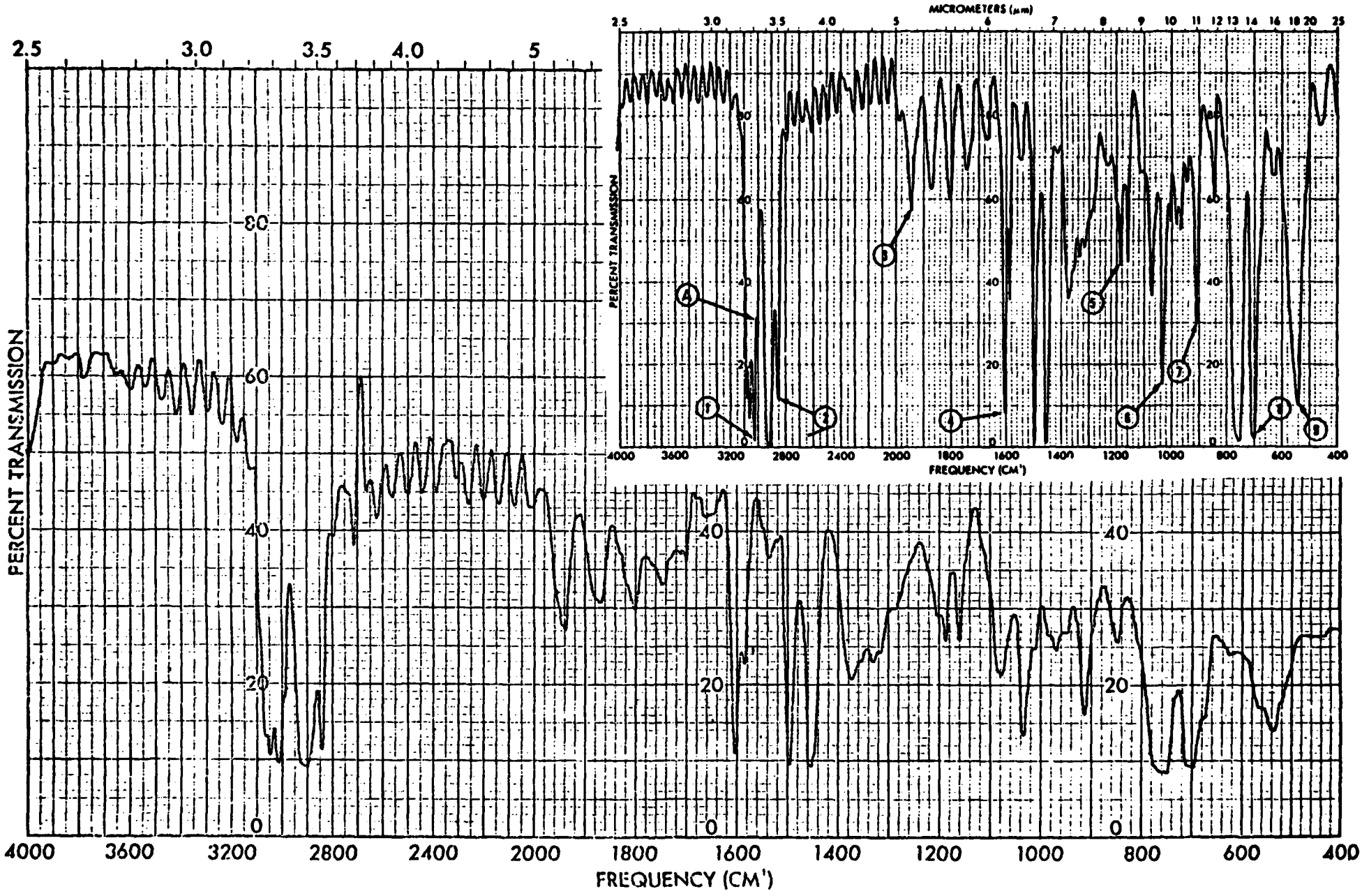
MICROMETERS (μm)
2.5
3.0
3.5
4.0
5
6
7
8
9
10
11
12
13
14
16
18
20
25
PERCENT TRANSMISSION
80
60
40
20
0
4000
3600
3200
2800
2400
2000
1800
1600
1400
1200
1000
800
600
400
FREQUENCY (CM')

Figure A-8. Single beam background spectrum with water vapor bands; calibrate mode with nothing in reference beam, and sample beam blocked. Inset: Same spectrum from Perkin-Elmer 735B instrument manual. CdTe transmission windows.

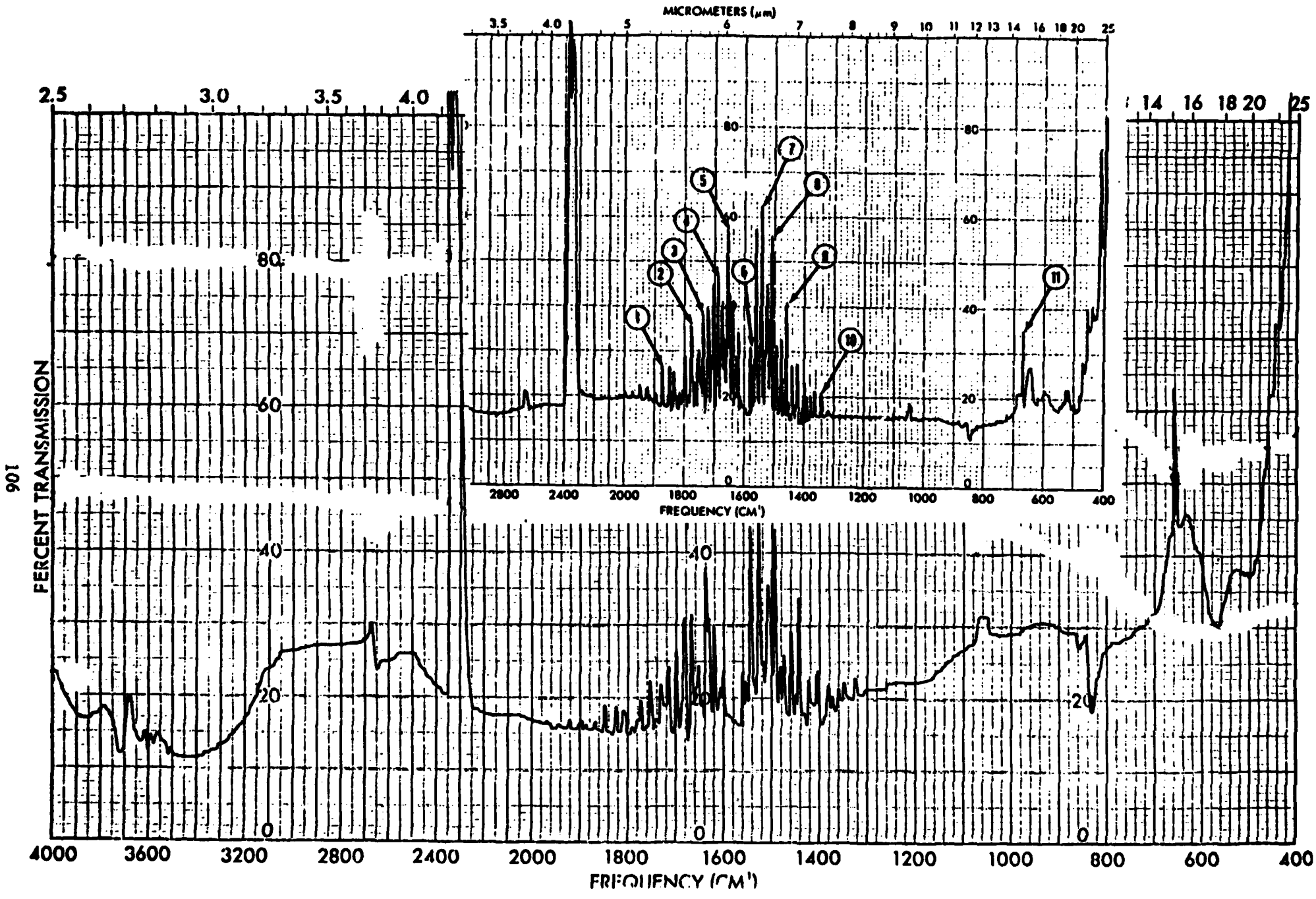
MICROMETERS (μm)
3.5 4.0 5 6 7 8 9 10 11 12 13 14 16 18 20 25
2.5 3.0 3.5 4.0
14 16 18 20 25
PERCENT TRANSMISSION
100
80
60
40
20
0
1 2 3 4 5 6 7 8 9 10 11
2800 2400 2000 1800 1600 1400 1200 1000 800 600 400
FREQUENCY (CM⁻¹)
4000 3600 3200 2800 2400 2000 1800 1600 1400 1200 1000 800 600 400
FREQUENCY (CM⁻¹)

Figure A-9. Schematic of the calibration apparatus for the ozonator.

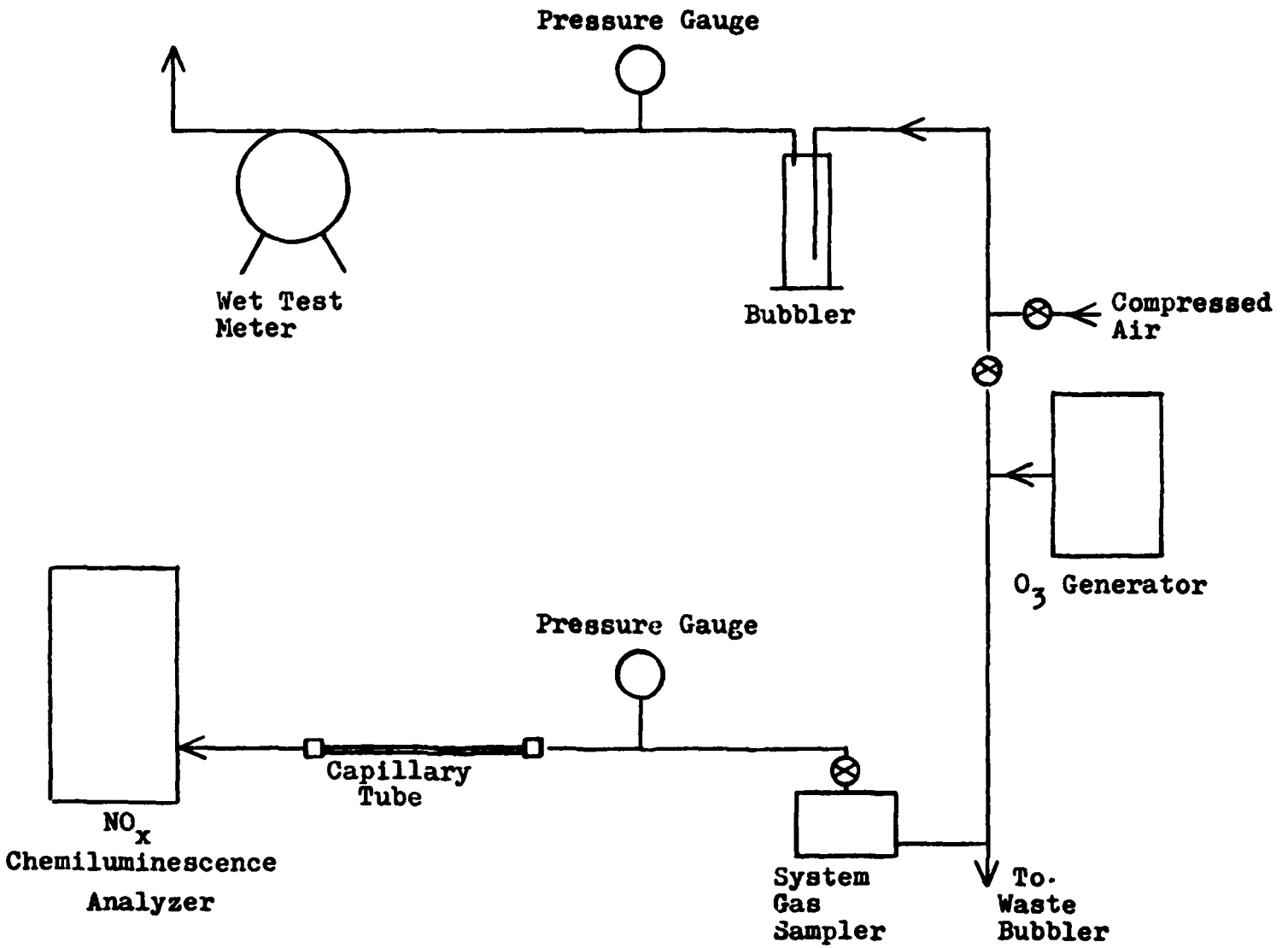
Pressure Gauge
Wet Test Meter
Bubbler
Compressed Air
O_3 Generator
Pressure Gauge
Capillary Tube
NO_x Chemiluminescence Analyzer
System Gas Sampler
To Waste Bubbler

APPENDIX B.

EXPERIMENTAL PROCEDURES

In this appendix, the general experimental procedures are summarized for deposition/formation of the cryofrost samples, and subsequent infrared and NO_x chemiluminescence analysis. The following descriptions make reference to the various parts of the experimental system as designated in Figure 1 of the text.

B.1. Sample line clean-up and cool-down.

1. First, the IR cell (i.e., the Excelon PVC vacuum shroud), the auxiliary cryopump (aluminum) shroud, and the sample lines were evacuated with a mechanical vacuum pump to < 1 mtorr.

2. After the entire system was evacuated, the auxiliary cryopump (i.e., the CS208L refrigerator) was be started. For experiments requiring a low water vapor background pressure, the system pumping was transferred to the auxiliary cryopump, after attaining operating temperature, by simply closing the foreline bellows valve.

3. After turning on the power to all the electrical equipment and allowing sufficient warmup time, the NO_x analyzer chamber and bypass pumps could be started, as well as the pure oxygen flow to the analyzer (@8 psig).

4. The infrared spectrophotometer was then set to monitor the condensed water vapor absorption peak at 3150 cm^{-1}, and the recorder was set to record the IR output and the temperature indicator. If additional water vapor deposition was desired, the liquid water reservoir was evacuated (with the foreline valve

closed), as well as the O_3/O_2 feed line, until the liquid was completely degassed.

B.2. Sample deposition and IR analysis.

1. With the sample feed lines purged and backfilled, and the fixed volume sample lines evacuated, the sample metering valves were fully closed and the sample lines were charged by opening the charging valves. Once the sample lines were filled, the charging valves were closed. The samples are then deposited on the cold window by slowing opening the metering valves; either individually, or simultaneously, depending on the specific type of experiment. The amount of sample actually deposited was calculated from the charge volume and pressure.

2. Infrared spectrophotometer scans could then be run as appropriate, depending on the specific experiment.

B.3. Flash desorption and NO_x analyzer mode.

1. The helium line pressure was set to -4 in. Hg, and the NO_x analyzer was flushed with helium. The strip chart recorder was zeroed to the output of the analyzer. The background suppression was set and the analyzer ozone generator was activated. The background levels in the NO and NO_x modes were recorded. The bypass flowrate was set to ~1.5 SCFM of air.

2. The foreline and auxiliary cryopump valves were closed. The sample window refriserator was turned off, and the heater was turned on (optional). The sample was then ready for desorption.

3. When the sample temperature attained 150K, the IR cell was backfilled with helium through the sample transfer line, using the transfer valve to meter in the helium at a low rate.

The analyzer bypass flowrate was watched to insure that it did not drop below 1.25 SCFM. When the IR cell pressure read -4 in. Hg, both the transfer valve and the purge valve at the rear of the IR cell shroud, were fully opened.

4. With the analyzer in the NO mode and recording a baseline, the helium bypass valve was closed. A mixture of the sample and the helium carrier gas then flowed through the transfer line. When the output peaked, the analyzer was quickly switched to the NO mode and the value recorded. Thereafter, the NO and NO_x modes were monitored alternately in order to record the decay curves for each mode. The corresponding peak areas were then calculated to establish the overall conversion for each experiment.

B.4. NO conversion calculations.

The experimental procedure for alternate recording of the NO and NO_x signals from the chemiluminescence analyzer result in peaks with an abrupt rise and a near-exponential decay. Thus, total amounts of NO and NO_x were determined by integrating the experimental response curves assuming:

$$C(t) = C_o \exp(Kt); \qquad (B-1)$$

the area of which is given by:

$$\text{Area} = \int_0^\infty C_o \exp(Kt) = -C_o/K \qquad (B-2)$$

A value of K was determined at each recorded data point. These were then averaged to yield the K value used in Eq. (B-2). In this manner, total signals in ppm-min were determined in the NO

and NO modes, which were then divided to yield $R=NO/NO_x$. The fractional conversion of NO is readily determined from:

$$x = R - R_o \qquad (B-3)$$

where $R=NO/NO_x$, and R_o is the value measured for the pure NO gas prior to deposition. This value remained approximately constant during the entire course of experimentation at about $R_o = 0.988$.

END

FILMED

3-84

DTIC